Published for SISSA by Springer

Received: *September 29, 2018*
Revised: *January 15, 2019*
Accepted: *January 21, 2019*
Published: *February 13, 2019*

Search for new physics in final states with a single photon and missing transverse momentum in proton-proton collisions at $\sqrt{s} = 13$ TeV



The CMS collaboration

E-mail: cms-publication-committee-chair@cern.ch

Abstract: A search is conducted for new physics in final states containing a photon and missing transverse momentum in proton-proton collisions at $\sqrt{s} = 13$ TeV, using the data collected in 2016 by the CMS experiment at the LHC, corresponding to an integrated luminosity of 35.9 fb^{-1}. No deviations from the predictions of the standard model are observed. The results are interpreted in the context of dark matter production and models containing extra spatial dimensions, and limits on new physics parameters are calculated at 95% confidence level. For the two simplified dark matter production models considered, the observed (expected) lower limits on the mediator masses are both 950 (1150) GeV for 1 GeV dark matter mass. For an effective electroweak-dark matter contact interaction, the observed (expected) lower limit on the suppression parameter Λ is 850 (950) GeV. Values of the effective Planck scale up to 2.85–2.90 TeV are excluded for between 3 and 6 extra spatial dimensions.

Keywords: Beyond Standard Model, Dark matter, Hadron-Hadron scattering (experiments)

ArXiv ePrint: 1810.00196

Open Access, Copyright CERN,
for the benefit of the CMS Collaboration.
Article funded by SCOAP[3].

https://doi.org/10.1007/JHEP02(2019)074

JHEP02(2019)074

Contents

1 Introduction 1

2 The CMS detector and event reconstruction 3

3 Event selection 5

4 Signal and background modeling 7

5 Background estimation 8
- 5.1 $Z(\rightarrow \nu\overline{\nu})+\gamma$ and $W(\rightarrow \ell\nu)+\gamma$ background 8
- 5.2 Electron misidentification background 11
- 5.3 Jet misidentification background 12
- 5.4 Beam halo and spikes background 12
- 5.5 Other minor SM background processes 13

6 Results 13
- 6.1 Signal extraction 13
- 6.2 Pre-fit and post-fit distributions 15
- 6.3 Limits 15

7 Summary 20

A Higher-order corrections to V+γ differential cross sections 22

B Simplified likelihood 22

The CMS collaboration 29

JHEP02(2019)074

1 Introduction

Production of events with a photon with large transverse momentum (p_T) and large missing transverse momentum (p_T^{miss}) at the CERN LHC is a sensitive probe of physics beyond the standard model (SM). This final state is often referred to as the "monophoton" signature, and has the advantage of being identifiable with high efficiency and purity. Among the extensions of the SM that can be studied with this final state are particle dark matter (DM) and large extra spatial dimensions.

At the LHC, the DM particles may be produced in high-energy proton-proton (pp) collisions, if they interact with the SM quarks or gluons via new couplings at the electroweak (EWK) scale [1–3]. Although DM particles cannot be directly detected, their production could be inferred from the observation of events with a large p_T imbalance, when high-energy SM particles recoil against the DM particle candidate. In DM production through a vector or axial-vector mediator, a photon can be radiated from the incident quarks (figure 1, left), resulting in a monophoton final state. In the simplified models considered

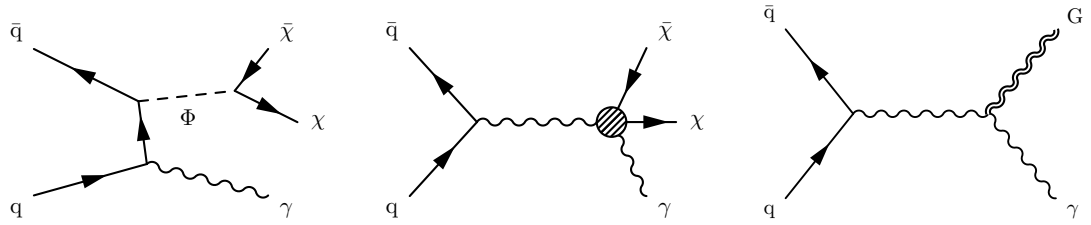


Figure 1. Leading order diagrams of the simplified DM model (left), EWK-DM effective interaction (center), and graviton (G) production in the ADD model (right), with a final state of a photon and large $p_{\mathrm{T}}^{\mathrm{miss}}$. Particles χ and $\overline{\chi}$ are the dark matter and its antiparticle, and Φ in the simplified DM model represents a vector or axial-vector mediator.

in this analysis, Dirac DM particles couple to a vector or axial-vector mediator, which in turn couples to the SM quarks. These models have been identified by the ATLAS-CMS Dark Matter Forum [4] as benchmarks to compare DM production sensitivity from various final states. They are characterized by a set of four parameters: the DM mass m_{DM}, the mediator mass M_{med}, the universal mediator coupling to quarks g_{q}, and the mediator coupling to DM particles g_{DM}. In this analysis, we fix the values of g_{q} and g_{DM} to 0.25 and 1.0, respectively, and scan the M_{med}–m_{DM} plane as recommended by the LHC Dark Matter Working Group [5].

It is also possible that the DM sector couples preferentially to the EWK sector, leading to an effective interaction $\mathrm{q\overline{q}} \to \mathrm{Z}/\gamma^* \to \gamma\chi\overline{\chi}$ [6], where χ is the DM particle (figure 1, center). This model is characterized by a set of four parameters: the DM mass m_{DM}, the suppression scale Λ, and the couplings k_1, k_2 to the U(1) and SU(2) gauge sectors, respectively. In this analysis, we fix the values of k_1 and k_2 to 1.0, and set limits on Λ at various values of m_{DM}.

The model of large extra dimensions proposed by Arkani-Hamed, Dimopoulos, and Dvali (ADD) [7, 8] postulates n extra spatial dimensions compactified at a characteristic scale R that reflects an effective Planck scale M_{D} through $M_{\mathrm{Pl}}^2 \approx M_{\mathrm{D}}^{n+2} R^n$, where M_{Pl} is the conventional Planck scale. If M_{D} is of the same order as the EWK scale ($M_{\mathrm{EWK}} \sim 10^2\,\mathrm{GeV}$), the large value of M_{Pl} can be interpreted as being a consequence of large-volume ($\sim R^n$) enhancement from extra dimensional space. This model predicts a process $\mathrm{q\overline{q}} \to \gamma\mathrm{G}$ (figure 1 right), where G represents one or more Kaluza-Klein gravitons, each of which can have any mass up to M_{D}. Since the gravitons escape detection, this process leads to the monophoton final state.

In this paper we describe a search for an excess of monophoton events over the SM prediction. Data collected by the CMS experiment in 2016, corresponding to an integrated luminosity of $35.9\,\mathrm{fb}^{-1}$, are analyzed. Results are interpreted in the context of the three processes represented in figure 1.

The primary irreducible background for the $\gamma + p_{\mathrm{T}}^{\mathrm{miss}}$ signal is the SM Z boson production associated with a photon, $\mathrm{Z}(\to \nu\overline{\nu})+\gamma$. Other SM background processes include $\mathrm{W}(\to \ell\nu)+\gamma$ (where the charged lepton ℓ escapes detection), $\mathrm{W} \to \ell\nu$ (where ℓ is misidentified as a photon), γ+jets, quantum chromodynamic (QCD) multijet events (with a jet misidentified as a photon), $\gamma\gamma$, $\mathrm{t}\gamma$, $\mathrm{t\bar{t}}\gamma$, $\mathrm{VV}\gamma$ (where V refers to a W or a Z boson), and

JHEP02(2019)074

$Z(\to \ell\bar{\ell})+\gamma$. Additionally, a small residual number of events from noncollision sources, such as beam halo [9] interactions and detector noise [10], contribute to the total background.

A similar search in pp collisions at $\sqrt{s} = 13\,\text{TeV}$, based on a data set corresponding to an integrated luminosity of $36.1\,\text{fb}^{-1}$, has been reported by the ATLAS experiment [11]. No significant excess over the SM prediction was observed. For the DM simplified model, a lower limit of 1200 GeV for both the vector and axial-vector mediator mass was set for low DM masses under the same assumption on the new-physics coupling values. For the EWK-DM effective interaction, a lower limit for the suppression parameter of the coupling was set at 790 GeV.

The previous search in the same final state by the CMS experiment [12] is based on $\sqrt{s} = 13\,\text{TeV}$ data corresponding to an integrated luminosity of $12.9\,\text{fb}^{-1}$, which is a subset of the data analyzed in this paper. In addition to benefiting from a larger sample size, the new analysis achieves improved sensitivity by using a simultaneous fit to the distributions of the p_T of the photon (E_T^γ) in various signal and control regions to estimate the signal contribution, rather than the "cut-and-count" method deployed previously.

The paper is organized as follows. The CMS detector apparatus is described in section 2, along with the algorithm used to reconstruct particles in pp collision events within the detector. Section 3 lists the requirements that events must pass in order to be selected for inclusion in the signal and control regions. Section 4 lists the Monte Carlo generators used to model various signal and background processes, and section 5 describes the methods used to estimate the expected background yields in the signal and control regions. These yields are tabulated in section 6, which also presents the limits obtained for each new physics model. The overall results are summarized in section 7. Appendix A gives a detailed description of the higher order corrections applied to the predicted differential cross sections of the leading background processes.

2 The CMS detector and event reconstruction

The central feature of the CMS apparatus is a superconducting solenoid of 6 m internal diameter, providing a magnetic field of 3.8 T. Within the solenoid volume are a silicon pixel and strip tracker, a lead tungstate crystal electromagnetic calorimeter (ECAL), and a brass and scintillator hadron calorimeter (HCAL), each composed of a barrel ($|\eta| < 1.48$) and two endcap ($1.48 < |\eta| < 3.00$) sections, where η is the pseudorapidity. The ECAL consists of 75 848 lead tungstate crystals, with 61 200 in the barrel and 7324 in each of the two endcaps. In the η–ϕ plane, HCAL cells in the barrel map on to 5×5 arrays of ECAL crystals to form calorimeter towers projecting radially outwards from close to the nominal interaction point. Forward calorimeters extend the η coverage provided by the barrel and endcap detectors. Muons are detected in gas-ionization chambers embedded in the steel flux-return yoke outside the solenoid.

Events of interest are selected using a two-level trigger system [13]. The first level, composed of custom hardware processors, uses information from the calorimeters and muon detectors to select events at a rate of around 100 kHz within a time interval of less than 4 μs. The second level, known as the high-level trigger (HLT), consists of a farm of processors

JHEP02(2019)074

running a version of the full event reconstruction software optimized for fast processing, and reduces the event rate to less than 1 kHz before data storage. A more detailed description of the CMS detector, together with a definition of the coordinate system and kinematic variables, can be found in ref. [14].

Global event reconstruction follows the particle-flow (PF) algorithm [15], which aims to reconstruct and identify each individual particle in an event with an optimized combination of all subdetector information. In this process, the identification of the particle type (photon, electron, muon, charged hadron, neutral hadron) plays an important role in the determination of the particle direction and energy. Photons are identified as ECAL energy clusters not linked to the extrapolation of any charged particle trajectory to the ECAL, while electrons are identified as ECAL energy clusters with such a link. Muons are identified as tracks in the central tracker consistent with either a track or several hits in the muon system, and associated with calorimeter deposits compatible with the muon hypothesis. Charged hadrons are identified as tracks neither identified as electrons nor as muons. Note that all three types of charged candidates can be associated to a reconstructed interaction vertex through their tracks. Finally, neutral hadrons are identified as HCAL energy clusters not linked to any charged hadron trajectory, or as ECAL and HCAL energy excesses with respect to the expected charged hadron energy deposit.

Reconstruction of pp interaction vertices proceeds from tracks using a deterministic annealing filter algorithm [16]. The reconstructed vertex with the largest value of summed physics-object p_{T}^2 is taken to be the primary pp interaction vertex. Here, the physics objects are the jets, clustered using the jet finding algorithm [17, 18] with the tracks assigned to the vertex as inputs, and the associated missing transverse momentum, taken as the negative vector sum of the p_{T} of those jets. These definitions of the jets and missing transverse momentum are specific to the context of vertex reconstruction, and are distinct from the definitions in the remainder of the analysis, as described in the following.

For each event, hadronic jets are clustered from these reconstructed PF candidates using the anti-k_{T} algorithm [17, 18] with a distance parameter of 0.4. The jet momentum is determined as the vector sum of all particle momenta in the jet. Because of the large number of additional pp interactions within the same or nearby bunch crossings (pileup), particles emerging from multiple interactions can be clustered into a jet. To mitigate this effect, charged candidates associated with vertices other than the primary one are discarded from clustering, and an offset correction is applied to the p_{T} of the jet to subtract the remaining contributions [19]. Jet energy corrections are derived from simulation to bring, on average, the measured response of jets to that of particle level jets. Measurements on data of the momentum balance in dijet, photon+jet, Z+jet, and multijet events are used to account for any residual differences in jet energy scale in data and simulation. Additional selection criteria are applied to each jet to remove jets potentially dominated by anomalous contributions from various subdetector components or reconstruction failures [19].

The missing transverse momentum vector ($\vec{p}_{\mathrm{T}}^{\,\mathrm{miss}}$) is defined as the negative vector sum of the transverse momenta of all PF candidates in an event. The magnitude of $\vec{p}_{\mathrm{T}}^{\,\mathrm{miss}}$ is the missing transverse momentum, $p_{\mathrm{T}}^{\mathrm{miss}}$.

ECAL clusters are identified starting from cluster seeds, which are ECAL crystals with energies above a minimum threshold, that must also exceed the energies of their immediate

JHEP02(2019)074

neighbors. Topological clusters are grown from seeds by adding adjacent crystals with energies above a lowered threshold, which could include other seeds. A topological cluster is finally separated into distinct clusters, one for each seed it contains, by fitting its energy distribution to a sum of Gaussian-distributed contributions from each seed.

Photon and electron reconstruction begins with the identification of ECAL clusters having little or no observed energy in the corresponding HCAL region. For each candidate cluster, the reconstruction algorithm searches for hits in the pixel and strip trackers that can be associated with the cluster. Such associated hits are called electron seeds, and are used to initiate a special track reconstruction based on a Gaussian sum filter [20, 21] which is optimized for electron tracks. The energy of electrons is determined from a combination of the electron momentum at the primary interaction vertex as determined by the tracker, the energy of the corresponding ECAL cluster, and the energy sum of all bremsstrahlung photons spatially compatible with originating from the electron track. An ECAL cluster with no associated electron seed, or with a significant energy excess relative to any compatible tracks, gives rise to a photon candidate. The energy of a photon is determined only from its corresponding ECAL cluster.

3 Event selection

The integrated luminosity of the analyzed data sample is $(35.9 \pm 0.9)\,\mathrm{fb}^{-1}$ [22]. The data sample is collected with a single-photon trigger that requires at least one photon candidate with $p_\mathrm{T} > 165\,\mathrm{GeV}$. The photon candidate must have $H/E < 0.1$ to discriminate against jets, where H/E is the ratio of HCAL to ECAL energy deposits in the central calorimeter tower corresponding to the candidate. The photon energy reconstructed at the HLT is less precise relative to that derived later in the offline reconstruction. Therefore, the thresholds in the trigger on both H/E and E_T^γ, are less restrictive than their offline counterparts. The trigger efficiency is measured to be about 98% for events passing the analysis selection with $E_\mathrm{T}^\gamma > 175\,\mathrm{GeV}$.

From the recorded data, events are selected by requiring $p_\mathrm{T}^\mathrm{miss} > 170\,\mathrm{GeV}$ and at least one photon with $E_\mathrm{T}^\gamma > 175\,\mathrm{GeV}$ in the fiducial region of the ECAL barrel ($|\eta| < 1.44$). Photon candidates are selected based on calorimetric information, isolation, and the absence of an electron seed, where the first two categories of the selection requirements are designed to discriminate the photon candidates from electromagnetic (EM) showers caused by hadrons, and the third is designed to discriminate photon candidates from electrons.

The calorimetric requirements for photons comprise $H/E < 0.05$ and $\sigma_{\eta\eta} < 0.0102$. The variable $\sigma_{\eta\eta}$, described in detail in ref. [23], represents the width of the EM shower in the η direction, which is generally larger in showers from hadronic activity. For a photon candidate to be considered as isolated, the scalar sums of the transverse momenta of charged hadrons, neutral hadrons, and photons within a cone of $\Delta R = \sqrt{(\Delta\eta)^2 + (\Delta\phi)^2} < 0.3$ around the candidate photon must all fall below a set of corresponding bounds chosen to give 80% signal efficiency. Only the PF candidates that do not overlap with the EM shower of the candidate photon are included in the isolation sums. Ideally, the isolation sum over PF charged hadrons should be computed using only the candidates sharing an

JHEP02(2019)074

interaction vertex with the photon candidate. However, because photon candidates are not reconstructed from tracks, their vertex association is ambiguous. When an incorrect vertex is assigned, nonisolated photon candidates can appear isolated. To reduce the rate for accepting nonisolated photon candidates, the maximum charged-hadron isolation value over all vertex hypotheses (worst isolation) is used. The above criteria select efficiently both unconverted photons and photons undergoing conversion in the detector material in front of the ECAL.

Stray ECAL clusters produced by mechanisms other than pp collisions can be misidentified as photons. In particular, anomalous ECAL energy deposits resulting from the interaction of particles in the ECAL photodetectors, from here on referred to as "ECAL spikes", as well as beam halo muons that accompany proton beams and penetrate the detector longitudinally have been found to produce spurious photon candidates at nonnegligible rates. The ECAL spike background is reduced by requiring that the photon candidate cluster must comprise more than a single ECAL crystal. To reject the beam halo induced EM showers, the ECAL signal in the seed crystal of the photon cluster is required to be within ± 3 ns of the arrival time expected for particles originating from a collision. In addition, the maximum of the total calorimeter energy summed along all possible paths of beam halo particles passing through the cluster (halo total energy), calculated for each photon candidate, must be below 4.9 GeV. The two requirements combined with the shower shape constraint suppress the beam halo background effectively, while retaining 95% of signal photons. Furthermore, using features described in section 5.4, the signal region is split into two parts according to ϕ to constrain the beam halo normalization. The region defined by $|\sin(\phi)| < \sin(0.5)$ is called the horizontal region, and its complement in ϕ is called the vertical region.

Events with a high-p_{T} photon and large $p_{\mathrm{T}}^{\mathrm{miss}}$ are subjected to further requirements to suppress SM background processes that feature a genuine high-energy photon, but not a significant amount of $p_{\mathrm{T}}^{\mathrm{miss}}$. One such SM process is γ+jets, where an apparent large $p_{\mathrm{T}}^{\mathrm{miss}}$ is often the result of a mismeasured jet energy. In contrast to signal processes, $p_{\mathrm{T}}^{\mathrm{miss}}$ is typically smaller than E_{T}^{γ} in these events, so requiring the ratio of E_{T}^{γ} to $p_{\mathrm{T}}^{\mathrm{miss}}$ to be less than 1.4 rejects this background effectively with little effect on signal efficiency. Events are also rejected if the minimum opening angle between $\vec{p}_{\mathrm{T}}^{\mathrm{miss}}$ and the directions of the four highest p_{T} jets, $\min\Delta\phi(\vec{p}_{\mathrm{T}}^{\mathrm{miss}}, \vec{p}_{\mathrm{T}}^{\mathrm{jet}})$, is less than 0.5. Only jets with $p_{\mathrm{T}} > 30$ GeV and $|\eta| < 5$ are considered in the $\min\Delta\phi(\vec{p}_{\mathrm{T}}^{\mathrm{miss}}, \vec{p}_{\mathrm{T}}^{\mathrm{jet}})$ calculation. In the γ+jets process, rare pathological mismeasurement of E_{T}^{γ} can also lead to large $p_{\mathrm{T}}^{\mathrm{miss}}$. For this reason, the candidate photon $\vec{p}_{\mathrm{T}}$ and $\vec{p}_{\mathrm{T}}^{\mathrm{miss}}$ must be separated by more than 0.5 radians. Another SM process to be rejected is $\mathrm{W}(\to \ell\nu)+\gamma$, for which events are vetoed if they contain an electron or a muon with $p_{\mathrm{T}} > 10$ GeV that is separated from the photon by $\Delta R > 0.5$.

The residual contributions from the $\mathrm{W}(\to \ell\nu)+\gamma$ process, where the lepton could not be identified or was out of the detector acceptance, are modeled by fitting to observed data, as described in section 5. The same method is employed to model the contribution from the $\mathrm{Z}(\to \nu\overline{\nu})+\gamma$ process to the signal region. This method utilizes control regions where one or two leptons (electrons or muons) are identified in addition to the photon, as defined in the following.

JHEP02(2019)074

The single-electron (single-muon) control region is defined by a requirement of exactly one electron (muon) with $p_{\mathrm{T}} > 30\,\mathrm{GeV}$ and $|\eta| < 2.5\,(2.4)$ in addition to a photon requirement that is identical to the one for the signal region. To suppress the contributions from large-$p_{\mathrm{T}}^{\mathrm{miss}}$ processes other than $\mathrm{W}(\to \ell\nu)+\gamma$, the transverse mass $\sqrt{2p_{\mathrm{T}}^{\mathrm{miss}}p_{\mathrm{T}}^{\ell}[1-\cos\Delta\phi(\vec{p}_{\mathrm{T}}^{\,\mathrm{miss}},\vec{p}_{\mathrm{T}}^{\,\ell})]}$ must be less than 160 GeV. Additionally, for the single-electron control region, $p_{\mathrm{T}}^{\mathrm{miss}}$ must be greater than 50 GeV to limit the contribution from the γ+jets process, where a jet is misidentified as an electron. Finally, the recoil vector $\vec{U} = \vec{p}_{\mathrm{T}}^{\,\mathrm{miss}} + \vec{p}_{\mathrm{T}}^{\,\ell}$, which serves as this region's analogue for $\vec{p}_{\mathrm{T}}^{\,\mathrm{miss}}$ in the signal region, must satisfy identical requirements to those for the $\vec{p}_{\mathrm{T}}^{\,\mathrm{miss}}$ in the signal region.

The dielectron (dimuon) control region is defined by exactly two electrons (muons) in addition to the photon, with $60 < m_{\ell\ell} < 120\,\mathrm{GeV}$, where $m_{\ell\ell}$ is the invariant mass of the dilepton system. The recoil vector of this region is $\vec{U} = \vec{p}_{\mathrm{T}}^{\,\mathrm{miss}} + \sum \vec{p}_{\mathrm{T}}^{\,\ell}$ and must satisfy identical requirements to those for the $\vec{p}_{\mathrm{T}}^{\,\mathrm{miss}}$ in the signal region.

4 Signal and background modeling

Monte Carlo simulation is used to model the signal and some classes of SM background events. For the leading order (LO) samples, the NNPDF3.0 [24] leading order (LO) parton distribution function (PDF) set is used with the strong coupling constant value $\alpha_S = 0.130$, whereas for the next-to-leading-order (NLO) samples, the NNPDF3.1 [25] next-to-next-to-leading-order (NNLO) PDF set with $\alpha_S = 0.118$ is employed. For the SM background processes, the primary hard interaction is simulated using the MadGraph5_aMC@NLO version 2.2.2 [26] generator at LO in QCD. The simulated events for the $\mathrm{Z}(\to \nu\overline{\nu})+\gamma$, $\mathrm{Z}(\to \ell\overline{\ell})+\gamma$, and $\mathrm{W}(\to \ell\nu)+\gamma$ background processes, collectively denoted as V+γ, are generated with MadGraph5_aMC@NLO at LO in QCD with up to two extra partons in the matrix element calculations. These are then normalized to the NLO EW and NNLO QCD cross sections using correction factors described in section 5. Parton showering and hadronization are provided by pythia 8.212 with the underlying-event tune CUETP8M1 [27]. Multiple simulated minimum bias events are overlaid on the primary interaction to model the distribution of pileup in data. Generated particles are processed through the full Geant4-based simulation of the CMS detector [28, 29].

For the DM signal hypotheses, MadGraph5_aMC@NLO 2.2.2 is used to produce MC simulation samples at NLO in QCD, requiring $E_{\mathrm{T}}^{\gamma} > 130\,\mathrm{GeV}$ and $|\eta^{\gamma}| < 2.5$. A large number of DM simplified model samples are generated, with varying M_{med} and m_{DM}. Similarly, EWK-DM effective interaction samples are generated in a range of 1–1000 GeV for the DM particle mass. For the ADD hypothesis, events are generated using pythia 8, requiring $E_{\mathrm{T}}^{\gamma} > 130\,\mathrm{GeV}$, with no restriction on the photon η. Samples are prepared in a grid of values for the number of extra dimensions and M_{D}. The efficiency of the full event selection for these signal models ranges between 0.06 and 0.29 for the DM simplified models, 0.44 and 0.46 for EW DM production, and 0.23 and 0.30 for the ADD model, depending on the parameters of the models.

JHEP02(2019)074

5 Background estimation

5.1 $Z(\to \nu\bar{\nu})+\gamma$ and $W(\to \ell\nu)+\gamma$ background

The most significant SM background processes in this search are the associated production of a high-energy γ with either a Z boson that subsequently decays to a pair of neutrinos, or a W boson that decays to a charged lepton and a neutrino. The two processes are denoted as $Z(\to \nu\bar{\nu})+\gamma$ and $W(\to \ell\nu)+\gamma$. Together, they account for approximately 70% of the SM background, with 50% from the former and 20% from the latter. Contributions from these two background processes are estimated using observed data in the four mutually exclusive single-electron, single-muon, dielectron, and dimuon control regions defined in section 3. The ratios between the expected yields of these processes are constrained by MC simulations of $V+\gamma$ processes.

The individual MC simulation samples of $V+\gamma$ processes receive multiple correction factors. First is the selection efficiency correction factor ρ, which accounts for subtle differences between simulation and observation in the reconstruction and identification efficiencies for various particle candidates. The value of ρ typically lies within a few percent of unity. The second factor is the higher-order QCD correction, which matches the distribution of the generator-level E_{T}^{γ} to that calculated at NNLO in QCD using the DYRes program [30]. The third factor further corrects the E_{T}^{γ} distributions to account for NLO EW effects, and is taken from refs. [31, 32], updated using the LUXqed17 PDF set [33].

Four sources of systematic uncertainties considered for E_{T}^{γ} distribution ratios among the $V+\gamma$ processes are PDFs, higher-order QCD corrections, higher-order EWK corrections, and data-to-simulation correction factors ρ. The PDF uncertainty is evaluated by varying the weight of each event using the weights provided in the NNPDF set, and taking the standard deviation of the resulting E_{T}^{γ} distributions. This uncertainty is considered fully correlated in the ratio between the $Z(\to \nu\bar{\nu})+\gamma$ and $W(\to \ell\nu)+\gamma$ processes, i.e., the variation of the ratio is bounded by the ratios of the upward and downward variations. Uncertainties related to higher-order QCD corrections are considered uncorrelated in the ratio between the $Z(\to \nu\bar{\nu})+\gamma$ and $W(\to \ell\nu)+\gamma$ processes. Because EW corrections become increasingly important at higher E_{T}^{γ}, but are known only up to NLO accuracy, their uncertainties are estimated by a special prescription similar to that discussed in ref. [34], where independent degrees of freedom are assigned to the uncertainty in the overall scale of the correction and the uncertainty in the variation of the correlation with E_{T}^{γ}. Additionally, the full correction due to photon-induced $Z+\gamma$ and $W+\gamma$ production cross sections is considered as an uncertainty. Further details concerning the higher-order QCD and EWK corrections are given in appendix A. Finally, data-to-simulation correction factors ρ for the lepton identification efficiencies have associated uncertainties that do not cancel when taking ratios between regions defined by different lepton selection requirements. The four uncertainties are all considered as correlated between the E_{T}^{γ} bins.

The background estimation method exploits cancellation of some of the systematic uncertainties, both experimental and theoretical, in the ratios of the photon E_{T}^{γ} distributions of $V+\gamma$ processes, from here on referred to as "transfer factors". For example, in the transfer factor between the $Z(\to \nu\bar{\nu})+\gamma$ and $Z(\to \ell\bar{\ell})+\gamma$ processes, denoted $R_{\ell\ell\gamma}^{\mathrm{Z}\gamma}$,

JHEP02(2019)074

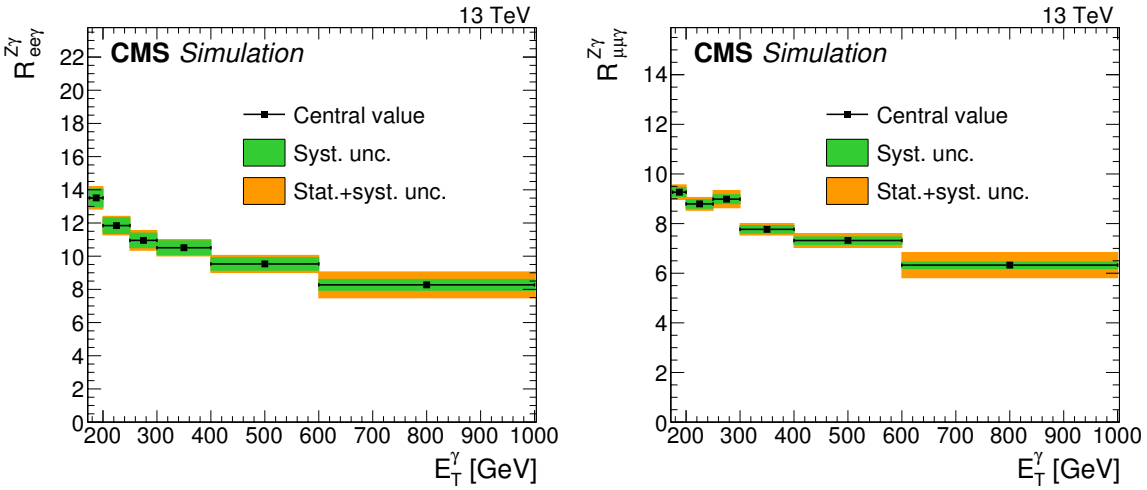


Figure 2. Transfer factors $R^{Z\gamma}_{ee\gamma}$ (left) and $R^{Z\gamma}_{\mu\mu\gamma}$ (right). The uncertainty bands in green (inner) and orange (outer) show the systematic uncertainty, and the combination of systematic and statistical uncertainty arising from limited MC sample size, respectively. The systematic uncertainties considered are the uncertainties in the data-to-simulation correction factors ρ for the lepton identification efficiencies. Simulated $Z(\to \ell\bar{\ell})+\gamma$ events are generated in two samples, one with generated E^{γ}_{T} required to be greater than 300 GeV, and one with a looser restriction. The E^{γ}_{T} bin centred at 270 GeV is close to the boundary between the two samples, where there are fewer generated events. The relatively large statistical fluctuation visible in the third bin of the right-hand figure results from this.

the uncertainties due to photon energy calibration, jet energy resolution, and higher-order QCD effects are significantly reduced compared to when such effects are considered for individual processes. The only uncertainties in the transfer factor $R^{Z\gamma}_{\ell\ell\gamma}$ that do not largely cancel are those on lepton identification efficiency and the statistical uncertainty due to the limited MC sample size. Figure 2 shows the transfer factor $R^{Z\gamma}_{ee\gamma}$ ($R^{Z\gamma}_{\mu\mu\gamma}$) between the dielectron (dimuon) control region and the combined signal regions, for which the numerator is the expected $Z(\to \nu\bar{\nu})+\gamma$ yield in the combined signal regions and the denominator is the expected $Z(\to \ell\bar{\ell})+\gamma$ yield in the relevant control region.

Using the transfer factor $R^{Z\gamma}_{\ell\ell\gamma}$, the total estimated event yield $T_{\ell\ell\gamma}$ in each dilepton control region in the i^{th} bin of the E^{γ}_{T} distribution can be expressed as

$$T_{\ell\ell\gamma,i} = \frac{N^{Z\gamma}_{i}}{R^{Z\gamma}_{\ell\ell\gamma,i}} + b_{\ell\ell\gamma,i}, \tag{5.1}$$

where $N^{Z\gamma}$ is the number of $Z(\to \nu\bar{\nu})+\gamma$ events in the combined signal regions and $b_{\ell\ell\gamma}$ is the predicted contribution from other background sources in the dilepton control region, namely $t\bar{t}\gamma$, $VV\gamma$, and misidentified hadrons. The subscript i indicates that the quantities are evaluated in bin i of the E^{γ}_{T} distribution.

Similar considerations apply to events arising from $W(\to \ell\nu)+\gamma$ processes. The charged lepton from these processes may either pass our identification criteria or fail, and in the ratio of these two classes of events, denoted $R^{W\gamma}_{\ell\gamma}$, the only uncertainties that remain non-

JHEP02(2019)074

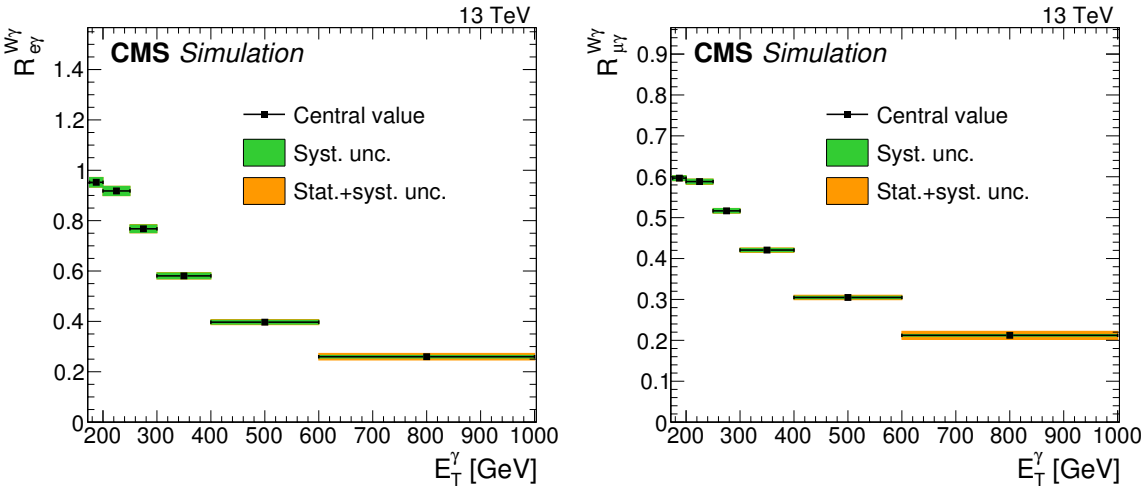


Figure 3. Transfer factors $R^{\mathrm{W}\gamma}_{\mathrm{e}\gamma}$ (left) and $R^{\mathrm{W}\gamma}_{\mu\gamma}$ (right). The uncertainty bands in green (inner) and orange (outer) show the systematic uncertainty, and the combination of systematic and statistical uncertainty arising from limited MC sample size, respectively. The systematic uncertainties considered are the uncertainties in the data-to-simulation correction factors ρ for the lepton identification efficiencies.

negligible are those associated with the lepton identification efficiency and the MC statistical uncertainty. Figure 3 shows the transfer factor $R^{\mathrm{W}\gamma}_{\mathrm{e}\gamma}$ ($R^{\mathrm{W}\gamma}_{\mu\gamma}$) between the single-electron (single-muon) control region and the combined signal regions, for which the numerator is the estimated $\mathrm{W}(\to \ell\nu)+\gamma$ yield in the combined signal regions, and the denominator is the estimated $\mathrm{W}(\to \ell\nu)+\gamma$ yield in the relevant control region.

Finally, an additional transfer factor $f^{\mathrm{Z}\gamma}_{\mathrm{W}\gamma} = N^{\mathrm{Z}\gamma}/N^{\mathrm{W}\gamma}$ is defined to connect the $\mathrm{Z}(\to \nu\overline{\nu})+\gamma$ and $\mathrm{W}(\to \ell\nu)+\gamma$ background yields in the signal regions, to benefit further from the larger statistical power that the single-lepton control samples provides. The quantity $N^{\mathrm{W}\gamma}$ is the number of $\mathrm{W}(\to \ell\nu)+\gamma$ events in the combined signal regions. When calculating the ratio $f^{\mathrm{Z}\gamma}_{\mathrm{W}\gamma}$, all experimental uncertainties associated with the data-to-simulation correction factors ρ cancel since both processes result in very similar event configurations. The main uncertainties in $f^{\mathrm{Z}\gamma}_{\mathrm{W}\gamma}$ are those from higher-order theoretical corrections. The relative magnitudes of the different theoretical uncertainties are shown in figure 13 in appendix A. Figure 4 shows the transfer factor $f^{\mathrm{Z}\gamma}_{\mathrm{W}\gamma}$ between the $\mathrm{Z}(\to \nu\overline{\nu})+\gamma$ and $\mathrm{W}(\to \ell\nu)+\gamma$ processes in the combined signal region. For every transfer factor described above, both the numerator and the denominator are estimated in MC.

For increasing E^{γ}_{T}, the Z boson in a $\mathrm{Z}(\to \ell\overline{\ell})+\gamma$ event tends to emerge with lower rapidity, and hence so do its decay products. As a consequence, the charged leptons are more likely to fall within the inner tracker acceptance, which increases the dilepton control region selection efficiency of these events. In contrast, the signal region selection efficiency of $\mathrm{Z}(\to \nu\overline{\nu})+\gamma$ events is unaffected by the rapidity of the final state neutrinos, as long as the observed $p^{\mathrm{miss}}_{\mathrm{T}}$ has the appropriate magnitude and azimuthal direction. This causes the distinctive drop in the ratio $R^{\mathrm{Z}\gamma}_{\ell\ell\gamma}$ with increasing E^{γ}_{T}. Similar arguments explain the drop in $R^{\mathrm{W}\gamma}_{\ell\gamma}$ as well as the rise in $f^{\mathrm{Z}\gamma}_{\mathrm{W}\gamma}$. The ratio $f^{\mathrm{Z}\gamma}_{\mathrm{W}\gamma}$ rises (rather than falls) with increasing

JHEP02(2019)074

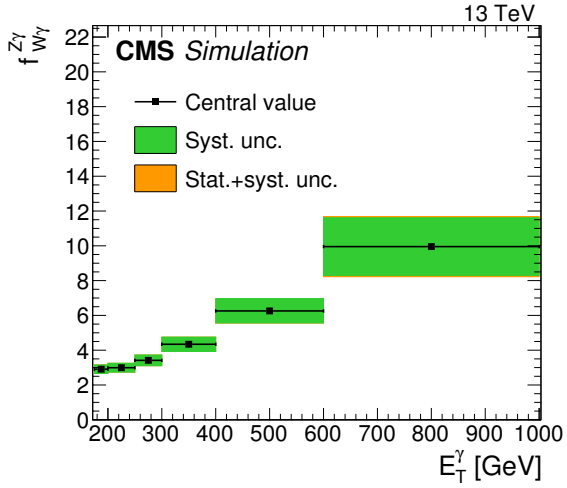


Figure 4. Transfer factor $f^{\mathrm{Z}\gamma}_{\mathrm{W}\gamma}$. The uncertainty bands in green (inner) and orange (outer) show the systematic uncertainty, and the combination of systematic and statistical uncertainty arising from limited MC sample size, respectively. The systematic uncertainties considered are the uncertainties from higher-order theoretical corrections.

E^{γ}_{T} because $\mathrm{W}(\to \ell\nu)+\gamma$ events have a lower (rather than higher) signal region selection efficiency if the charged lepton falls within the tracker acceptance.

Using $R^{\mathrm{W}\gamma}_{\ell\gamma}$ and $f^{\mathrm{Z}\gamma}_{\mathrm{W}\gamma}$, the total estimated event yield $T_{\ell\gamma}$ in each single-lepton control region in the ith bin of the E^{γ}_{T} distribution can be expressed as

$$T_{\ell\gamma,i} = \frac{N^{\mathrm{Z}\gamma}_{i}}{R^{\mathrm{W}\gamma}_{\ell\gamma,i} f^{\mathrm{Z}\gamma}_{\mathrm{W}\gamma,i}} + b_{\ell\gamma,i}, \tag{5.2}$$

where $b_{\ell\gamma}$ is the predicted contribution from other background sources in the single-lepton regions, namely misidentified electrons and hadrons and other minor SM processes.

5.2 Electron misidentification background

An important background consists of $\mathrm{W} \to \mathrm{e}\nu$ events in which the electron is misidentified as a photon. The misidentification occurs because of an inefficiency in seeding electron tracks. A seeding efficiency of ϵ for electrons with $p_{\mathrm{T}} > 160\,\mathrm{GeV}$ is measured in data using a tag-and-probe [35] technique in $\mathrm{Z} \to \mathrm{ee}$ events, and is validated with MC simulation. Misidentified electron events are modeled by a proxy sample of electron events, defined in data by requiring an ECAL cluster with a pixel seed. The proxy events must otherwise pass the same criteria used to select signal candidate events. The number of electron proxy events is then scaled by $R_{\epsilon} = (1-\epsilon)/\epsilon$ to yield an estimated contribution of events from electron misidentification to our signal candidate selection. The ratio R_{ϵ} was measured to be 0.0303 ± 0.0022 and uniform across the considered E^{γ}_{T} spectrum, with the dominant uncertainty in this estimate coming from the statistical uncertainty in the measurement of ϵ.

JHEP02(2019)074

5.3 Jet misidentification background

Electromagnetic showers from hadronic activity can also mimic a photon signature. This process is estimated by counting the numbers of events in two different subsets of a low-$p_{\mathrm{T}}^{\mathrm{miss}}$ multijet data sample. The first subset consists of events with a photon candidate that satisfies the signal selection criteria. These events contain both genuine photons and jets that are misidentified as photons. The second subset comprises events with a candidate photon that meets less stringent shower shape requirements and inverted isolation criteria with respect to the signal candidates. Nearly all of the candidate photons in these events arise from jet misidentification. The hadron misidentification ratio is defined as the ratio between the number of misidentified events in the first subset to the total number of events in the second subset.

The numerator is estimated by fitting the observed shower shape distribution of the photon candidate in the first subset with a combination of simulated distributions and distributions obtained from the observed data. For genuine photons, the shower width distribution is formed using simulated γ+jets events. For jets misidentified as photons, the distribution is obtained from a sample selected by inverting the charged-hadron isolation and removing the shower-shape requirement entirely.

The hadron misidentification ratio is measured to be between 0.08 and 0.12 with a few percent relative uncertainty depending on the energy of the photon candidate. The dominant uncertainty is systematic, and comprises the shower shape distribution fit and shower shape modelling uncertainty, along with uncertainties associated with variations in the charged hadron isolation threshold, low-$p_{\mathrm{T}}^{\mathrm{miss}}$ requirement, and template bin width.

The final estimate of the contribution of jet misidentification background to our signal candidate selection is computed by multiplying the hadron misidentification ratio by the number of events in the high-$p_{\mathrm{T}}^{\mathrm{miss}}$ control sample with a photon candidate that satisfies the conditions used to select the second subset of the low-$p_{\mathrm{T}}^{\mathrm{miss}}$ control sample.

5.4 Beam halo and spikes background

Estimates of beam halo background and spike background are derived from fits of the angular and timing distributions of the calorimeter clusters. Energy clusters in the ECAL due to beam halo muons are observed to concentrate around $|\sin(\phi)| \sim 0$, while all other processes (collision-related processes and ECAL spikes) produce photon candidates that are uniformly distributed in ϕ [9], motivating the splitting of the signal region introduced in section 3.

The splitting of the signal region can be thought of as a two-bin fit. Collision processes occupy the relative fractions of phase space in the horizontal (H) and vertical (V) signal regions, $C_H = 1/\pi$ and $C_V = (\pi - 1)/\pi$, respectively. The corresponding fractions for beam halo events are determined by selecting a halo-enriched sample where the halo identification is inverted. Thus, a fit of the two signal regions provides an estimate of the overall normalization of the beam halo background, denoted h. The E_{T}^{γ} dependence of the halo background is encoded in $n_{K,i}^{\mathrm{halo}}$, the unit-normalized beam halo prediction in bin i of the signal region $K \in \{H, V\}$. Using the notation introduced in section 5.1, the total

JHEP02(2019)074

E_{T}^{γ} [GeV]	[175, 200]	[200, 250]	[250, 300]	[300, 400]	[400, 600]	[600, 1000]
$\mathrm{Z}\gamma$	81.2 ± 8.0	88.2 ± 8.4	38.8 ± 4.8	26.8 ± 3.7	8.8 ± 1.9	1.4 ± 0.7
$\mathrm{W}\gamma$	27.9 ± 3.7	29.9 ± 3.9	11.4 ± 1.7	6.3 ± 1.2	1.4 ± 0.4	0.1 ± 0.1
Misid. electrons	22.5 ± 2.7	25.7 ± 2.7	10.5 ± 1.0	8.2 ± 0.7	2.7 ± 0.2	0.5 ± 0.0
Misid. hadrons	5.2 ± 2.2	9.3 ± 1.8	3.1 ± 0.7	1.0 ± 0.3	0.4 ± 0.1	0.0 ± 0.0
Other SM	13.6 ± 2.0	19.6 ± 1.3	13.9 ± 0.4	4.2 ± 0.2	0.8 ± 0.0	0.1 ± 0.0
ECAL spikes	4.3 ± 1.3	2.7 ± 0.8	0.5 ± 0.1	0.1 ± 0.0	0.0 ± 0.0	0.0 ± 0.0
Total prediction	154.6 ± 8.3	175.4 ± 8.8	78.2 ± 5.3	46.6 ± 4.0	14.1 ± 2.1	2.1 ± 0.8
Observed	150 ± 12	166 ± 13	76.0 ± 8.7	44.0 ± 6.6	19.0 ± 4.4	4.0 ± 2.0

Table 1. Expected event yields in each E_{T}^{γ} bin for various background processes in the horizontal signal region. The background yields and the corresponding uncertainties are obtained after performing a combined fit to data in all the control samples, excluding data in the signal region. The observed event yields in the horizontal signal region are also reported.

estimated background T_K in the two signal regions are

$$\begin{aligned} T_{K,i} &= C_K(N_i^{\mathrm{Z}\gamma} + N_i^{\mathrm{W}\gamma}) + hn_{K,i}^{\mathrm{halo}} + C_K b_{K,i} \\ &= C_K(1 + {f_{\mathrm{W}\gamma i}^{\mathrm{Z}\gamma}}^{-1})N_i^{\mathrm{Z}\gamma} + hn_{K,i}^{\mathrm{halo}} + C_K b_{K,i}, \end{aligned}$$

where $b_{K,i}$ is the total contribution to bin i of region K from electron and hadron misidentification, ECAL spikes, and other minor SM background processes.

The distribution of the cluster seed timing provides a cross-check on the beam halo background estimate and an independent means to estimate the ECAL spikes contribution [10]. A three-component fit of the cluster seed timing using the halo, spike, and prompt-photon templates are performed. The timing distribution of the spike background is obtained by inverting the lower bound on the shower shape requirement in the candidate photon selection. A total spike background of 22.9 ± 5.8 events is predicted, where the dominant uncertainty is statistical.

5.5 Other minor SM background processes

The SM $\mathrm{t\bar{t}}\gamma$, $\mathrm{VV}\gamma$, $\mathrm{Z}(\to \ell\bar{\ell})+\gamma$, $\mathrm{W} \to \ell\nu$, and γ+jets processes are minor ($\sim$10%) background processes in the signal region. Although $\mathrm{Z}(\to \ell\bar{\ell})+\gamma$ and γ+jets do not involve high-p_{T} invisible particles, the former can exhibit large $p_{\mathrm{T}}^{\mathrm{miss}}$ when the leptons fail to be reconstructed, and the latter when jet energy is severely mismeasured. The estimates for all five processes are taken from MadGraph5_aMC@NLO simulations at LO in QCD and can be found in tables 1 and 2.

6 Results

6.1 Signal extraction

The potential signal contribution is extracted from the data via simultaneous fits to the E_{T}^{γ} distributions in the signal and control regions. Uncertainties in various quantities are

JHEP02(2019)074

E_{T}^{γ} [GeV]	[175, 200]	[200, 250]	[250, 300]	[300, 400]	[400, 600]	[600, 1000]
$\mathrm{Z}\gamma$	172 ± 17	190 ± 18	83 ± 10	58.6 ± 7.9	18.0 ± 3.9	3.1 ± 1.6
$\mathrm{W}\gamma$	59.9 ± 7.8	63.6 ± 7.8	24.6 ± 3.5	13.4 ± 2.4	3.0 ± 0.8	0.3 ± 0.2
Misid. electrons	48.4 ± 5.6	56.2 ± 5.1	23.4 ± 1.8	15.7 ± 1.4	5.6 ± 0.4	1.2 ± 0.1
Misid. hadrons	15.1 ± 4.4	14.5 ± 3.1	4.2 ± 0.8	2.3 ± 0.8	0.5 ± 0.1	0.1 ± 0.1
Other SM	33.8 ± 4.1	36.6 ± 2.7	13.6 ± 0.5	17.1 ± 0.6	2.4 ± 0.1	0.8 ± 0.0
ECAL spikes	9.3 ± 2.8	5.7 ± 1.7	0.9 ± 0.3	0.3 ± 0.1	0.0 ± 0.0	0.0 ± 0.0
Total prediction	339 ± 18	366 ± 19	150 ± 11	107.5 ± 8.7	29.6 ± 4.3	5.4 ± 1.7
Observed	301	342	161	107	41.0	12.0

Table 2. Expected event yields in each E_{T}^{γ} bin for various background processes in the vertical signal region. The background yields and the corresponding uncertainties are obtained after performing a combined fit to data in all the control samples, excluding data in the signal regions. The observed event yields in the vertical signal region are also reported.

represented by nuisance parameters in the fit. Predictions for $\mathrm{Z}(\to \nu\overline{\nu})+\gamma$, $\mathrm{W}(\to \ell\nu)+\gamma$, and the beam halo backgrounds are varied in the fit. Beam halo is not a major background, but the extraction of its rate requires a fit to the observed distributions in the signal region.

Free parameters of the fit are the yield of $\mathrm{Z}(\to \nu\overline{\nu})+\gamma$ background in each bin of the signal regions ($N_i^{\mathrm{Z}\gamma}$) and the overall normalization of the beam halo background (h). Bin-by-bin yields of $\mathrm{W}(\to \ell\nu)+\gamma$ and $\mathrm{Z}(\to \ell\overline{\ell})+\gamma$ samples in all regions are related to the yield of $\mathrm{Z}(\to \nu\overline{\nu})+\gamma$ through the MC prediction through the transfer factors defined in section 5.1. The transfer factors are allowed to shift within the aforementioned theoretical and experimental uncertainties.

The background-only likelihood that is maximized in the fit is

$$
\begin{aligned}
\mathcal{L} &= \prod_i \left\{\mathcal{L}_{\text{signal}}\, \mathcal{L}_{\text{single-lepton}}\, \mathcal{L}_{\text{dilepton}}\right\}\, \mathcal{L}_{\text{nuisances}} \\
&= \prod_i \left\{ \prod_{K=H,V} \mathcal{P}\left(d_{K,i} \left| T_{K,i}\left(\vec{\theta}\right)\right.\right) \prod_{\ell=\mathrm{e},\mu} \mathcal{P}\left(d_{\ell\gamma,i} \left| T_{\ell\gamma,i}\left(\vec{\theta}\right)\right.\right) \prod_{\ell=\mathrm{e},\mu} \mathcal{P}\left(d_{\ell\ell\gamma,i} \left| T_{\ell\ell\gamma,i}\left(\vec{\theta}\right)\right.\right) \right\} \prod_j \mathcal{N}(\theta_j) \\
&= \prod_i \left\{ \begin{array}{l} \displaystyle\prod_{K=H,V} \mathcal{P}\left(d_{K,i} \left| \left(1 + f_{\mathrm{W}\gamma,i}^{\mathrm{Z}\gamma\ -1}\left(\vec{\theta}\right)\right) C_K N_i^{\mathrm{Z}\gamma} + h n_{K,i}^{\text{halo}}\left(\vec{\theta}\right) + C_K b_{K,i}\left(\vec{\theta}\right)\right.\right) \\ \qquad \times \displaystyle\prod_{\ell=\mathrm{e},\mu} \mathcal{P}\left(d_{\ell\gamma,i} \left| \frac{N_i^{\mathrm{Z}\gamma}}{R_{\ell\gamma,i}^{\mathrm{W}\gamma}\left(\vec{\theta}\right) f_{\mathrm{W}\gamma,i}^{\mathrm{Z}\gamma}\left(\vec{\theta}\right)} + b_{\ell\gamma,i}\left(\vec{\theta}\right)\right.\right) \\ \qquad \times \displaystyle\prod_{\ell=\mathrm{e},\mu} \mathcal{P}\left(d_{\ell\ell\gamma,i} \left| \frac{N_i^{\mathrm{Z}\gamma}}{R_{\ell\ell\gamma,i}^{\mathrm{Z}\gamma}\left(\vec{\theta}\right)} + b_{\ell\ell\gamma,i}\left(\vec{\theta}\right)\right.\right) \end{array} \right\} \prod_j \mathcal{N}(\theta_j),
\end{aligned}
$$

following the notation introduced in section 5, and where $\mathcal{P}(n|\lambda)$ is the Poisson probability of n for mean λ, $\mathcal{N}$ denotes the unit normal distribution, and $d_{X,i}$ is the observed number of events in bin i of region X. Systematic uncertainties are treated as nuisance parameters in the fit and are represented by $\vec{\theta}$. Each quantity Q_j with a nominal value $\overline{Q}_j$ and a standard deviation of the systematic uncertainty σ_j appears in the likelihood function as $\overline{Q}_j \exp(\sigma_j \theta_j)$.

JHEP02(2019)074

The systematic uncertainties considered in this analysis, including the ones already mentioned in section 5, are:

- Theoretical uncertainties in V+γ differential cross sections, incorporated as uncertainties on the transfer factors (see section 5.1)
- Uncertainties in trigger efficiency and photon and lepton identification efficiencies
- Electron and jet misidentification rate uncertainties (see sections 5.2 and 5.3)
- Photon and jet energy scale uncertainties (see refs. [36] and [19])
- Beam halo and ECAL spike rate and distribution uncertainties (see section 5.4)
- Minor SM background cross section uncertainties
- Uncertainty in integrated luminosity (see ref. [22])

Of the listed uncertainties, only the first two categories have a significant impact on the result of the signal extraction fit.

6.2 Pre-fit and post-fit distributions

Figure 5 shows the observed E_{T}^{γ} distributions in the four control regions compared with the results from simulations before and after performing the simultaneous fit across all the control samples and signal region, and assuming absence of any signal. Figure 6 shows the observed E_{T}^{γ} distributions in the horizontal and vertical signal regions compared with the results from simulations before and after performing a combined fit to the data in all the control samples and the signal region. The observed distributions are in agreement with the prediction from SM and noncollision backgrounds. In particular, the fit estimates the beam halo background to be zero in both regions. The dominant systematic uncertainties in the signal model include those on the integrated luminosity, jet and γ energy scales, $p_{\mathrm{T}}^{\mathrm{miss}}$ resolution, and data-to-simulation scale factors discussed in section 5.

The expected yields in each bin of E_{T}^{γ} for all backgrounds in the horizontal and vertical signal regions after performing a combined fit to data in all the control samples, excluding data in the signal regions, are given in tables 1 and 2, respectively. The covariances between the predicted background yields across all the E_{T}^{γ} bins in the two signal regions are shown in figure 15 in appendix A. The expected yields together with the covariances can be used with the simplified likelihood approach detailed in ref. [37] to reinterpret the results for models not studied in this paper.

6.3 Limits

No significant excess of events beyond the SM expectation is observed. Upper limits are determined for the production cross section of three new-physics processes mentioned in section 1. For each model, a 95% confidence level (CL) upper limit is obtained utilizing the asymptotic $\mathrm{CL_s}$ criterion [38–40], using a test statistic based on the negative logarithm of the likelihood in section 6.1.

JHEP02(2019)074

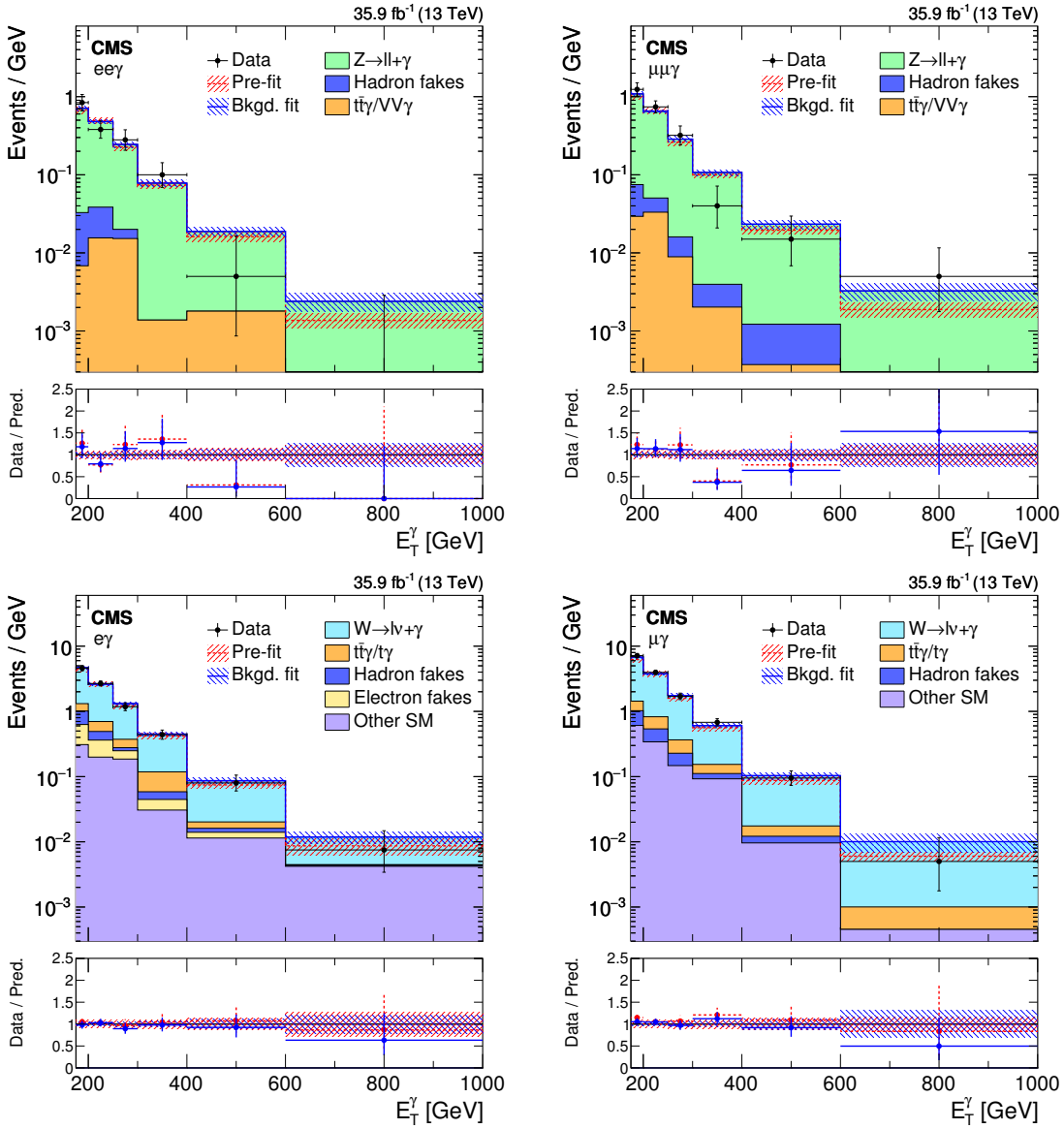


Figure 5. Comparison between data and MC simulation in the four control regions: eeγ (upper left), $\mu\mu\gamma$ (upper right), eγ (lower left), $\mu\gamma$ (lower right) before and after performing the simultaneous fit across all the control samples and signal region, and assuming absence of any signal. The last bin of the distribution includes all events with $E_{\mathrm{T}}^{\gamma} > 1000\,\mathrm{GeV}$. The ratios of data with the pre-fit background prediction (red dashed) and post-fit background prediction (blue solid) are shown in the lower panels. The bands in the lower panels show the post-fit uncertainty after combining all the systematic uncertainties.

The simplified DM models parameters proposed by the ATLAS-CMS Dark Matter Forum [4] are designed to facilitate the comparison and translation of various DM search results. Figure 7 shows the 95% CL upper cross section limits with respect to the corresponding theoretical cross section ($\mu_{95} = \sigma_{95\%}/\sigma_{\mathrm{theory}}$) for the vector and axial-vector mediator scenarios, in the M_{med}–m_{DM} plane. The solid black (dashed red) curves are the observed (expected) contours of $\mu_{95} = 1$. The σ_{theory} hypothesis is excluded at 95% CL or

JHEP02(2019)074

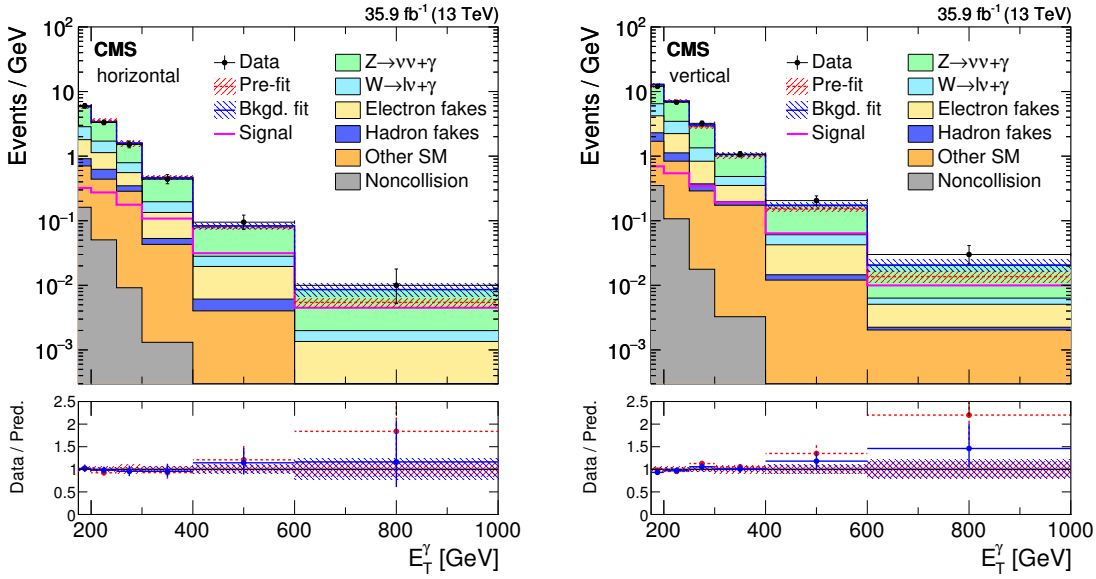


Figure 6. Observed E_{T}^{γ} distributions in the horizontal (left) and vertical (right) signal regions compared with the post-fit background expectations for various SM processes. The last bin of the distribution includes all events with $E_{\mathrm{T}}^{\gamma} > 1000\,\mathrm{GeV}$. The expected background distributions are evaluated after performing a combined fit to the data in all the control samples and the signal region. The ratios of data with the pre-fit background prediction (red dashed) and post-fit background prediction (blue solid) are shown in the lower panels. The bands in the lower panels show the post-fit uncertainty after combining all the systematic uncertainties. The expected signal distribution from a 1 TeV vector mediator decaying to 1 GeV DM particles is overlaid.

above in the region with $\mu_{95} < 1$. The uncertainty in the expected upper limit includes the experimental uncertainties. For the simplified DM LO models considered, mediator masses up to 950 GeV are excluded for values of m_{DM} less than 1 GeV.

The results for vector, axial-vector, and pseudoscalar mediators are compared to constraints from the observed cosmological relic density of DM as determined from measurements of the cosmic microwave background by the Planck satellite experiment [41]. The expected DM abundance is estimated, separately for each model, using the thermal freeze-out mechanism implemented in the MadDM [42] framework and compared to the observed cold DM density $\Omega_c h^2 = 0.12$ [41], where Ω_c is the DM relic abundance and h is the dimensionless Hubble constant.

The exclusion contours in figure 7 are also translated into the $\sigma_{\mathrm{SI/SD}}$–m_{DM} plane, where $\sigma_{\mathrm{SI/SD}}$ are the spin-independent/spin-dependent DM-nucleon scattering cross sections as shown in figure 8. The translation and presentation of the result follows the prescription given in ref. [5]. In particular, to enable a direct comparison with results from direct detection experiments, these limits are calculated at 90% CL [4]. When compared to the direct detection experiments, the limits obtained from this search provide stronger constraints for DM masses less than 2 GeV (spin independent) and less than 200 GeV (spin dependent).

For the DM model with a contact interaction of type $\gamma\gamma\chi\overline{\chi}$, upper limits are placed on the production cross section, which are then translated into lower limits on the suppression

JHEP02(2019)074

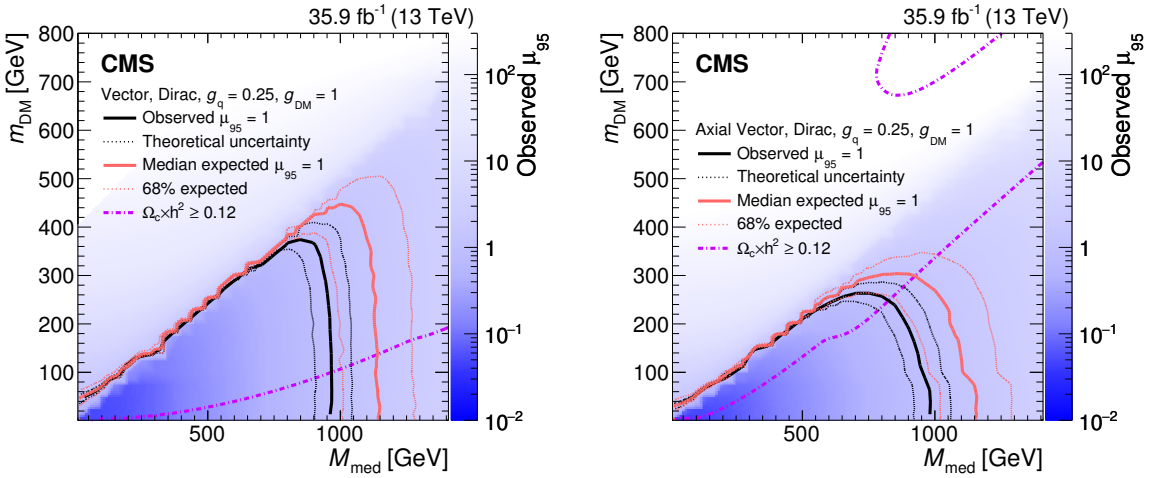


Figure 7. The ratio of 95% CL upper cross section limits to the theoretical cross section (μ_{95}), for DM simplified models with vector (left) and axial-vector (right) mediators, assuming $g_q = 0.25$ and $g_{DM} = 1$. Expected $\mu_{95} = 1$ contours are overlaid in red. The region under the observed contour is excluded. For DM simplified model parameters in the region below the lower violet dot-dash contour, and also above the corresponding upper contour in the right hand plot, cosmological DM abundance exceeds the density observed by the Planck satellite experiment.

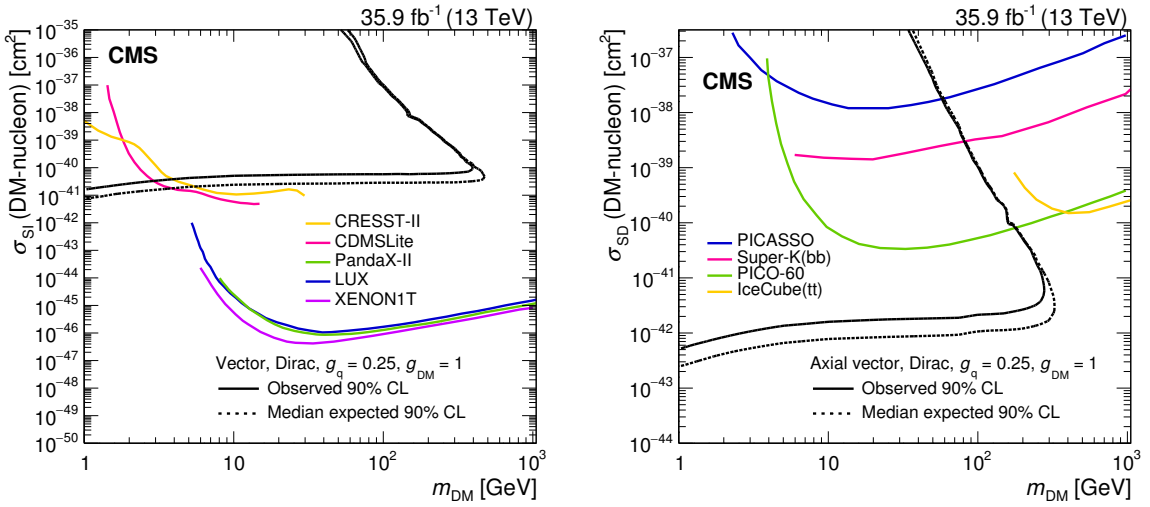


Figure 8. The 90% CL exclusion limits on the χ-nucleon spin-independent (left) and spin-dependent (right) scattering cross sections involving vector and axial-vector operators, respectively, as a function of the m_{DM}. Simplified model DM parameters of $g_q = 0.25$ and $g_{DM} = 1$ are assumed. The region to the upper left of the contour is excluded. On the plots, the median expected 90% CL curve overlaps the observed 90% CL curve. Also shown are corresponding exclusion contours, where regions above the curves are excluded, from the recent results by CDMSLite [43], LUX [44], PandaX-II [45], XENON1T [46], CRESST-II [47], PICO-60 [48], IceCube [49], PICASSO [50] and Super-Kamiokande [51] collaborations.

JHEP02(2019)074

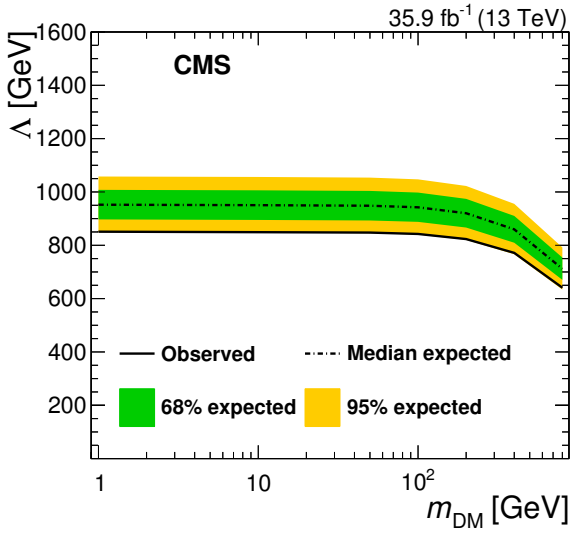


Figure 9. The 95% CL observed and expected lower limits on Λ for an effective EWK-DM contact interaction, as a function of dark matter mass m_{DM}.

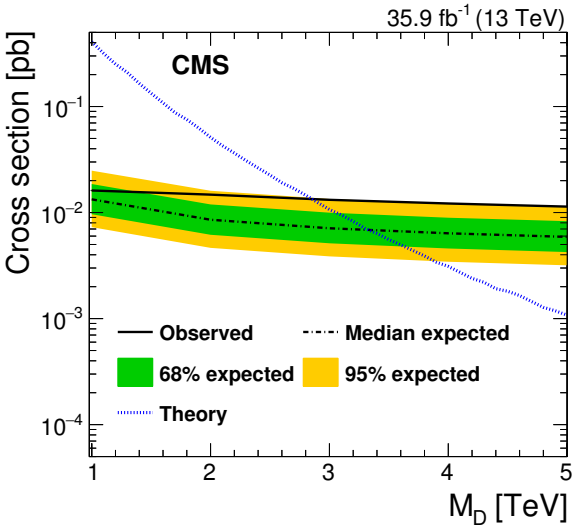


Figure 10. The 95% CL upper limits on the ADD graviton production cross section as a function of M_{D}, for $n = 3$ extra dimensions.

scale Λ for $k_1 = k_2 = 1.0$. The 95% CL observed and expected lower limits on Λ as a function of dark matter mass m_{DM} are shown in figure 9. For m_{DM} between 1 and 100 GeV, we exclude Λ values up to 850 (950) GeV, observed (expected) at 95% CL.

Figure 10 shows the upper limit and the theoretically calculated ADD graviton production cross section for $n = 3$ extra dimensions, as a function of M_{D}. Lower limits on M_{D} for various values of n extra dimensions are summarized in table 3, and in figure 11. Values of M_{D} up to 2.90 TeV for $n = 6$ are excluded by the current analysis.

The sensitivity of the analysis to new physics, as measured by the stringency of the expected cross section upper limits, has improved by approximately 70% in comparison

JHEP02(2019)074

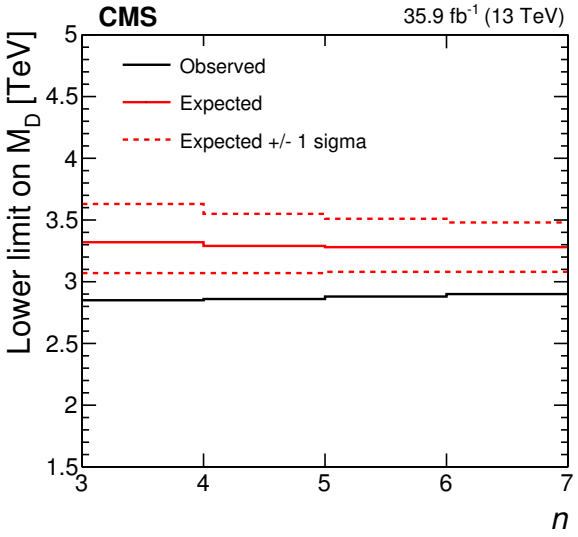


Figure 11. Lower limit on M_{D} as a function of n, the number of ADD extra dimensions.

n	Obs. limit [TeV]	Exp. limit [TeV]
3	2.85	3.32
4	2.86	3.29
5	2.88	3.28
6	2.90	3.28

Table 3. The 95% CL observed and expected lower limits on M_{D} as a function of n, the number of ADD extra dimensions.

to the previous CMS results [12]. A threefold increase in the data set size accounts for one fourth of the improvement, with the rest of the gain resulting from by the use of the simultaneous fit to multiple signal and control regions.

7 Summary

Proton-proton collisions producing a high transverse momentum photon and large missing transverse momentum have been investigated to search for new phenomena, using a data set corresponding to $35.9\,\mathrm{fb}^{-1}$ of integrated luminosity recorded at $\sqrt{s} = 13\,\mathrm{TeV}$ at the LHC. An analysis strategy of performing a simultaneous fit to multiple signal and control regions is employed on this final state for the first time, enhancing the sensitivity to potential signal events. No deviations from the standard model predictions are observed. For the simplified dark matter production models considered, the observed (expected) lower limit on the mediator mass is 950 (1150) GeV in both cases for 1 GeV dark matter mass. For an effective electroweak-dark matter contact interaction, the observed (expected) lower limit on the suppression parameter Λ is 850 (950) GeV. For the model with extra spatial dimensions, values of the effective Planck scale M_{D} up to 2.85–2.90 TeV are excluded for between 3 and 6 extra dimensions. These limits on Λ and M_{D} are the most sensitive monophoton limits to date.

JHEP02(2019)074

Acknowledgments

We congratulate our colleagues in the CERN accelerator departments for the excellent performance of the LHC and thank the technical and administrative staffs at CERN and at other CMS institutes for their contributions to the success of the CMS effort. In addition, we gratefully acknowledge the computing centers and personnel of the Worldwide LHC Computing Grid for delivering so effectively the computing infrastructure essential to our analyses. Finally, we acknowledge the enduring support for the construction and operation of the LHC and the CMS detector provided by the following funding agencies: BMBWF and FWF (Austria); FNRS and FWO (Belgium); CNPq, CAPES, FAPERJ, FAPERGS, and FAPESP (Brazil); MES (Bulgaria); CERN; CAS, MoST, and NSFC (China); COLCIENCIAS (Colombia); MSES and CSF (Croatia); RPF (Cyprus); SENESCYT (Ecuador); MoER, ERC IUT, and ERDF (Estonia); Academy of Finland, MEC, and HIP (Finland); CEA and CNRS/IN2P3 (France); BMBF, DFG, and HGF (Germany); GSRT (Greece); NKFIA (Hungary); DAE and DST (India); IPM (Iran); SFI (Ireland); INFN (Italy); MSIP and NRF (Republic of Korea); MES (Latvia); LAS (Lithuania); MOE and UM (Malaysia); BUAP, CINVESTAV, CONACYT, LNS, SEP, and UASLP-FAI (Mexico); MOS (Montenegro); MBIE (New Zealand); PAEC (Pakistan); MSHE and NSC (Poland); FCT (Portugal); JINR (Dubna); MON, RosAtom, RAS, RFBR, and NRC KI (Russia); MESTD (Serbia); SEIDI, CPAN, PCTI, and FEDER (Spain); MOSTR (Sri Lanka); Swiss Funding Agencies (Switzerland); MST (Taipei); ThEPCenter, IPST, STAR, and NSTDA (Thailand); TUBITAK and TAEK (Turkey); NASU and SFFR (Ukraine); STFC (United Kingdom); DOE and NSF (U.S.A.).

Individuals have received support from the Marie-Curie program and the European Research Council and Horizon 2020 Grant, contract No. 675440 (European Union); the Leventis Foundation; the A.P. Sloan Foundation; the Alexander von Humboldt Foundation; the Belgian Federal Science Policy Office; the Fonds pour la Formation à la Recherche dans l'Industrie et dans l'Agriculture (FRIA-Belgium); the Agentschap voor Innovatie door Wetenschap en Technologie (IWT-Belgium); the F.R.S.-FNRS and FWO (Belgium) under the "Excellence of Science — EOS" — be.h project n. 30820817; the Ministry of Education, Youth and Sports (MEYS) of the Czech Republic; the Lendület ("Momentum") Program and the János Bolyai Research Scholarship of the Hungarian Academy of Sciences, the New National Excellence Program ÚNKP, the NKFIA research grants 123842, 123959, 124845, 124850 and 125105 (Hungary); the Council of Science and Industrial Research, India; the HOMING PLUS program of the Foundation for Polish Science, cofinanced from European Union, Regional Development Fund, the Mobility Plus program of the Ministry of Science and Higher Education, the National Science Center (Poland), contracts Harmonia 2014/14/M/ST2/00428, Opus 2014/13/B/ST2/02543, 2014/15/B/ST2/03998, and 2015/19/B/ST2/02861, Sonata-bis 2012/07/E/ST2/01406; the National Priorities Research Program by Qatar National Research Fund; the Programa Estatal de Fomento de la Investigación Científica y Técnica de Excelencia María de Maeztu, grant MDM-2015-0509 and the Programa Severo Ochoa del Principado de Asturias; the Thalis and Aristeia programs cofinanced by EU-ESF and the Greek NSRF; the Rachadapisek Sompot Fund for

JHEP02(2019)074

Postdoctoral Fellowship, Chulalongkorn University and the Chulalongkorn Academic into Its 2nd Century Project Advancement Project (Thailand); the Welch Foundation, contract C-1845; and the Weston Havens Foundation (U.S.A.).

A Higher-order corrections to V+γ differential cross sections

In order to account for higher-order electroweak corrections, we apply additional factors as a function of E_{T}^{γ}. Of the various electroweak higher-order effects, ones that can give sizeable ($\gg \mathcal{O}(\alpha)$) corrections to the differential cross section are Sudakov suppression at high photon p_{T} and potentially the addition of photon-induced scattering processes [31, 32]. We apply the correction factors shown in figure 12, which are combinations of Sudakov suppression factors and photon-induced enhancements, and are provided by the authors of ref. [32] in addition to the NNLO QCD correction.

The differential cross section after the full higher-order corrections is therefore denoted as

$$\mathrm{d}\sigma^{\text{NNLO QCD+NLO EW}} = \mathrm{d}\sigma^{\mathrm{LO}} k^{\text{NNLO QCD}} (1 + \kappa^{\text{EW Sudakov}} + \kappa^{\text{EW q}\gamma}), \tag{A.1}$$

where $k^{\text{NNLO QCD}} = \mathrm{d}\sigma^{\text{NNLO QCD}}/\mathrm{d}\sigma^{\mathrm{LO}}$, and the two κ terms are the Sudakov suppression and photon-induced enhancement components of the electroweak correction, respectively.

We estimate the magnitude of the uncertainty in $\kappa^{\text{EW Sudakov}}$ and $\kappa^{\text{EW q}\gamma}$ to be $(\kappa^{\text{EW Sudakov}})^2$ and $\kappa^{\text{EW q}\gamma}$, i.e., square of the correction for Sudakov suppression and the 100% of the correction itself for the photon-induced enhancement. The choice of using the square of $\kappa^{\text{EW Sudakov}}$ is motivated by the fact that fully resummed leading-log Sudakov suppression is an exponential of $\kappa^{\text{EW Sudakov}}$.

For the Sudakov suppression, which is the dominant term in the electroweak correction, we further consider two types of systematic variations, inspired by ref. [34], which provides a prescription for electroweak correction uncertainties for V+jets processes. In that paper, electroweak correction as a function of the boson p_{T} is varied in overall scale and in slope. The slope variation is realized by selecting a point in the boson p_{T} spectrum and letting the shift in correction cross over at the point.

Figure 13 shows the effect of systematic uncertainty in the ratio between the $\mathrm{Z}(\to \nu\bar{\nu})+\gamma$ and $\mathrm{W}(\to \ell\nu)+\gamma$ processes with respect to nominal value for $\mathrm{Z}\gamma$ and $\mathrm{W}\gamma$ respectively.

B Simplified likelihood

Figure 14 shows the comparison between data and the post-fit background predictions in the horizontal and vertical signal regions, where the background prediction is obtained from a combined fit performed in all control regions, excluding the signal regions. The covariances between the predicted background yields across all the E_{T}^{γ} bins in the two signal regions are shown in figure 15.

Additionally, table 4 shows the step-by-step efficiency of various selections for the irreducible $\mathrm{Z}\gamma$ and $\mathrm{W}\gamma$ processes as well as two representative signal models.

JHEP02(2019)074

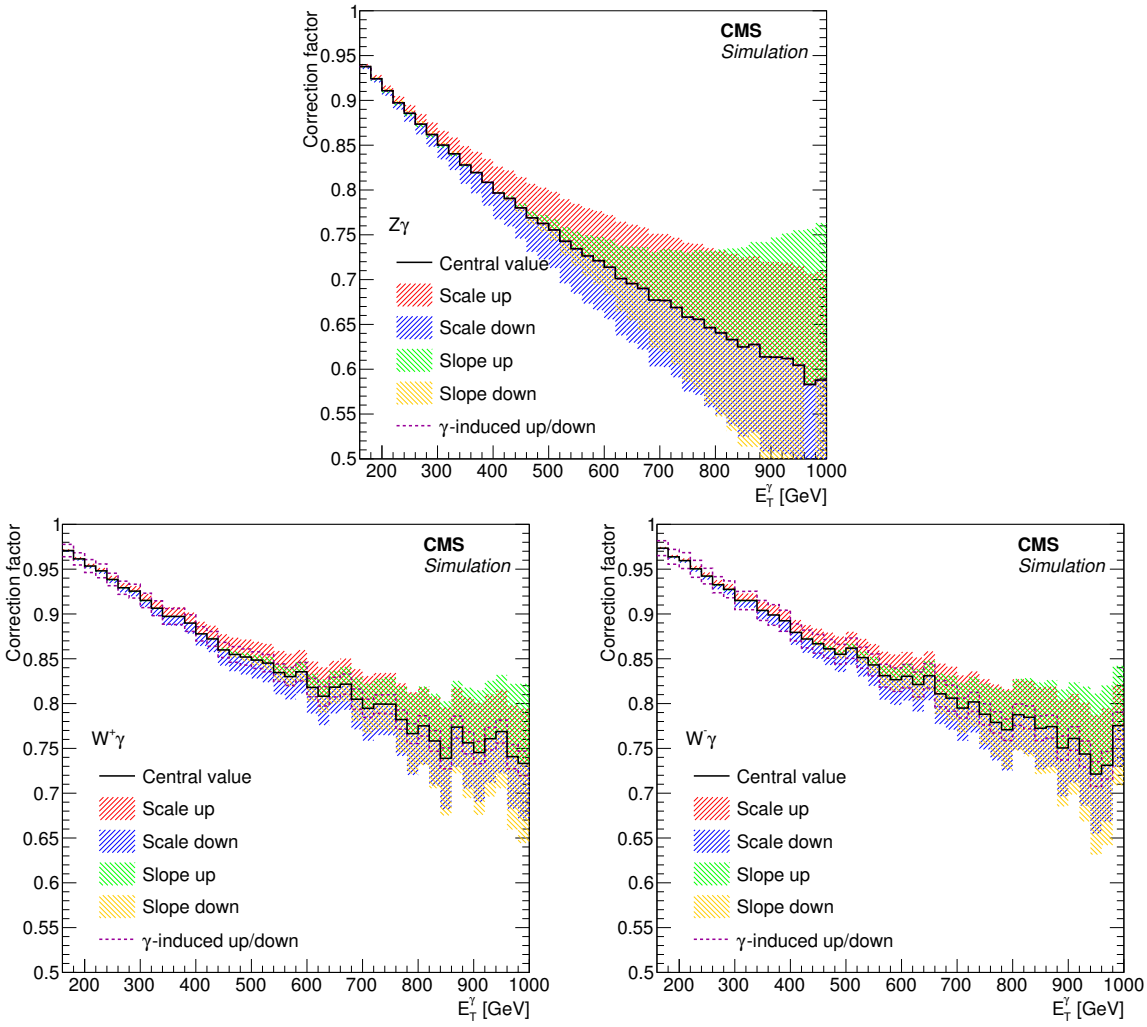


Figure 12. Electroweak NLO cross section corrections as a function of photon p_T for $Z(\to \nu\bar{\nu})+\gamma$ (top), $W^+ + \gamma$ (bottom left), and $W^- + \gamma$ (bottom right) processes, overlaid with uncertainty bands. See text for descriptions of the individual components of the uncertainty. Uncertainty due to γ-induced production is negligible in $Z(\to \nu\bar{\nu})+\gamma$ production.

	Zγ	Wγ	Vector mediator	ADD graviton
Trigger	0.4498	0.4750	0.6348	0.6610
Photon selection	0.1832	0.1960	0.3194	0.3664
$p_T^{miss} > 170\,GeV$	0.1064	0.0297	0.2800	0.3305
Lepton veto	0.1055	0.0148	0.2781	0.3283
$\Delta\phi(p_T^{miss}, \gamma) > 0.5$	0.1047	0.0134	0.2271	0.3283
$\min\Delta\phi(\vec{p}_T^{miss}, \vec{p}_T^{jet}) > 0.5$	0.0928	0.0084	0.2512	0.3004
$E_T^\gamma/p_T^{miss} < 1.4$	0.0892	0.0074	0.2477	0.2959

Table 4. Step-by-step efficiencies of various selections for irreducible Zγ and Wγ processes as well as two representative signal models: a 1 TeV vector mediator decaying to 1 GeV DM particles and an ADD graviton model with 8 extra dimensions and $M_D = 3$ TeV. The statistical uncertainties on these values are generally on the order of half a percent.

JHEP02(2019)074

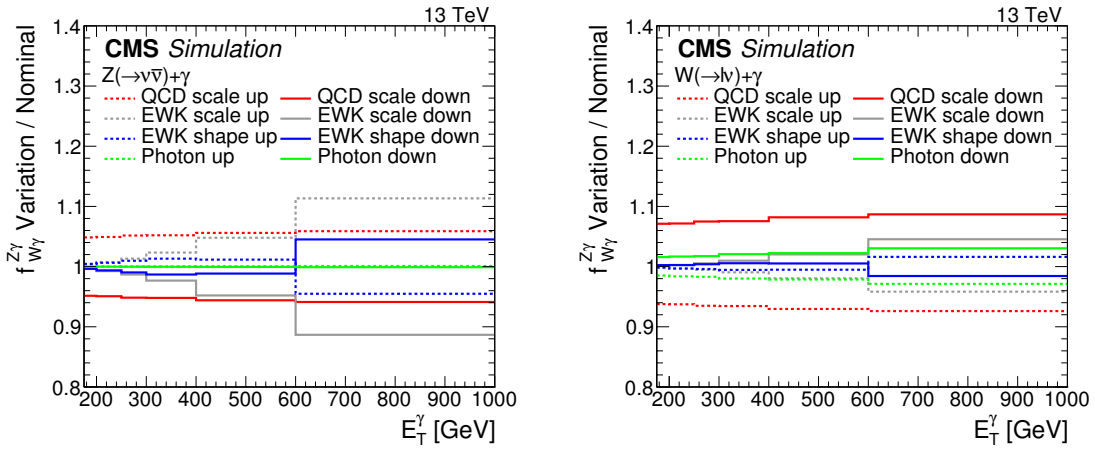


Figure 13. Systematic uncertainty in the transfer factors for $\mathrm{Z}(\to \nu\bar{\nu})+\gamma$ (left) and $\mathrm{W}(\to \ell\nu)+\gamma$ (right). The last bin includes all events with $E_\mathrm{T}^\gamma > 1000\,\mathrm{GeV}$.

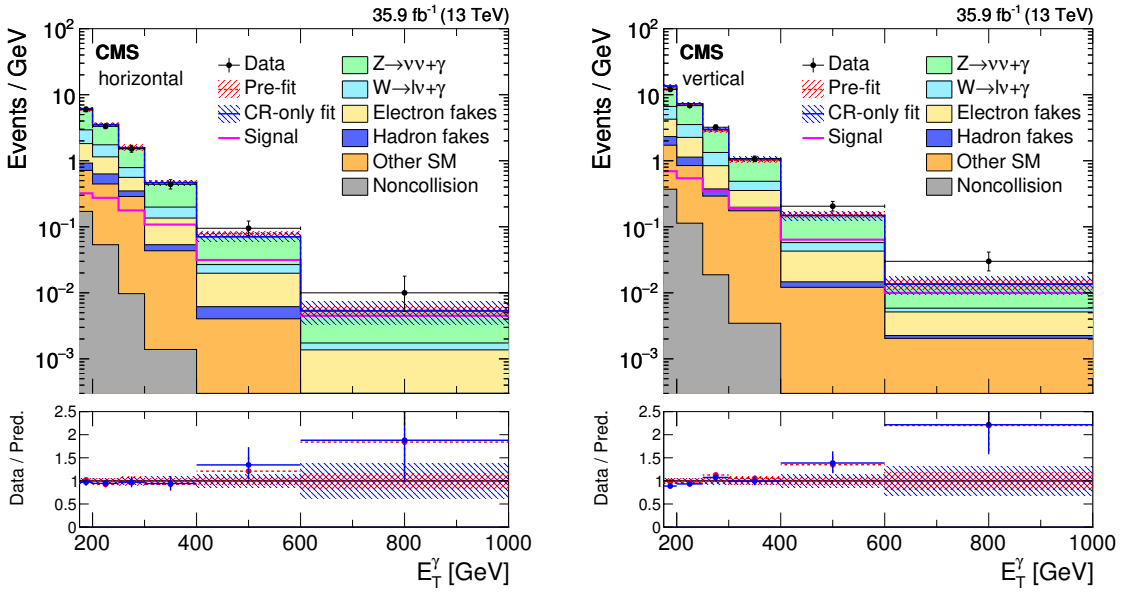


Figure 14. Observed E_T^γ distribution in the horizontal (left) and vertical (right) signal regions compared with the post-fit background expectations for various SM processes. The last bin includes all events with $E_\mathrm{T}^\gamma > 1000\,\mathrm{GeV}$. The expected background distributions are evaluated after performing a combined fit to the data in all the control samples, not including the signal region.

JHEP02(2019)074

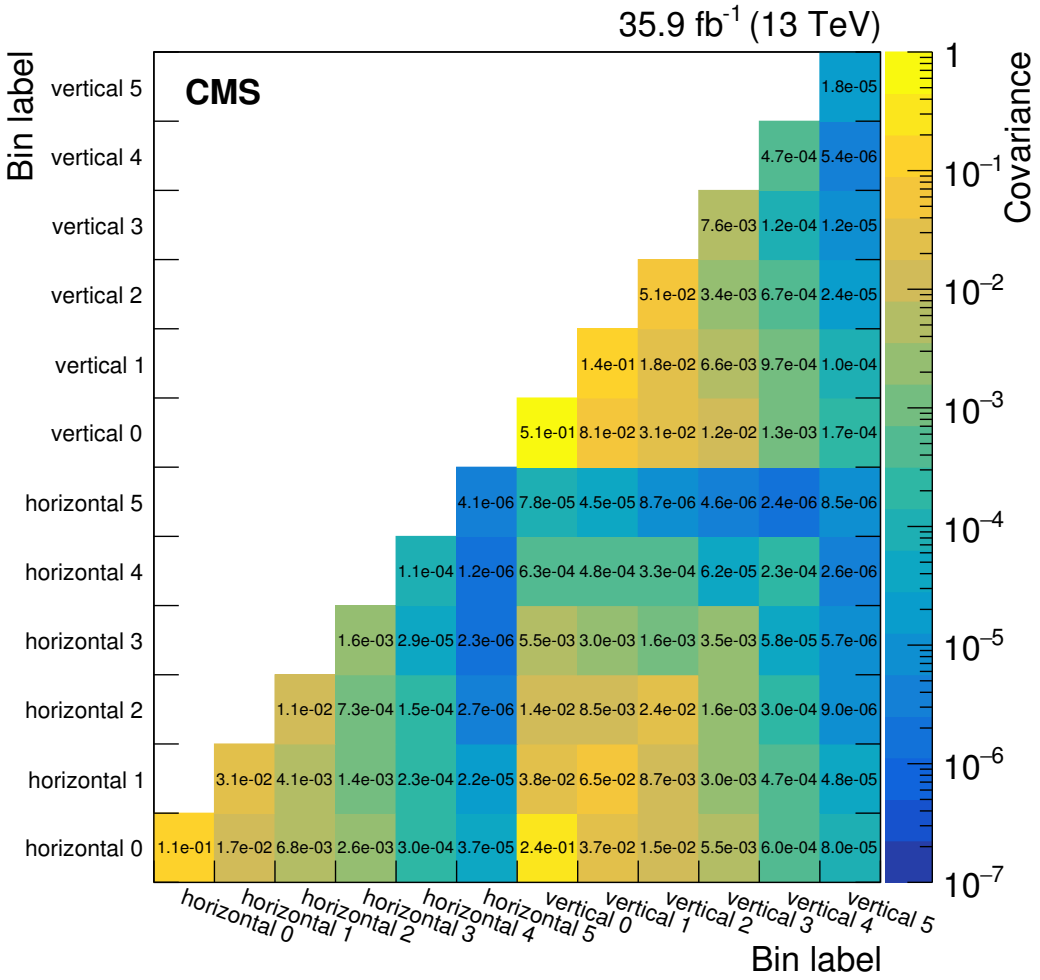


Figure 15. Covariances between the predicted background yields in all the E_{T}^{γ} bins of the horizontal and vertical signal regions. The bin labels specify which signal region the bin belongs to and what number bin it is for that region.

Open Access. This article is distributed under the terms of the Creative Commons Attribution License (CC-BY 4.0), which permits any use, distribution and reproduction in any medium, provided the original author(s) and source are credited.

References

[1] M. Beltrán, D. Hooper, E.W. Kolb, Z.A.C. Krusberg and T.M.P. Tait, *Maverick dark matter at colliders*, *JHEP* **09** (2010) 037 [arXiv:1002.4137] [INSPIRE].

[2] J. Goodman, M. Ibe, A. Rajaraman, W. Shepherd, T.M.P. Tait and H.-B. Yu, *Constraints on Dark Matter from Colliders*, *Phys. Rev.* **D 82** (2010) 116010 [arXiv:1008.1783] [INSPIRE].

[3] P.J. Fox, R. Harnik, J. Kopp and Y. Tsai, *Missing Energy Signatures of Dark Matter at the LHC*, *Phys. Rev.* **D 85** (2012) 056011 [arXiv:1109.4398] [INSPIRE].

[4] D. Abercrombie et al., *Dark Matter Benchmark Models for Early LHC Run-2 Searches: Report of the ATLAS/CMS Dark Matter Forum*, arXiv:1507.00966 [INSPIRE].

JHEP02(2019)074

[5] G. Busoni et al., *Recommendations on presenting LHC searches for missing transverse energy signals using simplified s-channel models of dark matter*, arXiv:1603.04156 [INSPIRE].

[6] A. Nelson, L.M. Carpenter, R. Cotta, A. Johnstone and D. Whiteson, *Confronting the Fermi Line with LHC data: an Effective Theory of Dark Matter Interaction with Photons*, *Phys. Rev.* **D 89** (2014) 056011 [arXiv:1307.5064] [INSPIRE].

[7] N. Arkani-Hamed, S. Dimopoulos and G.R. Dvali, *The Hierarchy problem and new dimensions at a millimeter*, *Phys. Lett.* **B 429** (1998) 263 [hep-ph/9803315] [INSPIRE].

[8] N. Arkani-Hamed, S. Dimopoulos and G.R. Dvali, *Phenomenology, astrophysics and cosmology of theories with submillimeter dimensions and TeV scale quantum gravity*, *Phys. Rev.* **D 59** (1999) 086004 [hep-ph/9807344] [INSPIRE].

[9] S. Orfanelli et al., *A novel Beam Halo Monitor for the CMS experiment at the LHC*, 2015 *JINST* **10** P11011 [INSPIRE].

[10] CMS collaboration, *Mitigation of anomalous APD signals in the CMS electromagnetic calorimeter*, *J. Phys. Conf. Ser.* **404** (2012) 012043 [INSPIRE].

[11] ATLAS collaboration, *Search for dark matter at* $\sqrt{s} = 13$ *TeV in final states containing an energetic photon and large missing transverse momentum with the ATLAS detector*, *Eur. Phys. J.* **C 77** (2017) 393 [arXiv:1704.03848] [INSPIRE].

[12] CMS collaboration, *Search for new physics in the monophoton final state in proton-proton collisions at* $\sqrt{s} = 13$ *TeV*, *JHEP* **10** (2017) 073 [arXiv:1706.03794] [INSPIRE].

[13] CMS collaboration, *The CMS trigger system*, 2017 *JINST* **12** P01020 [arXiv:1609.02366] [INSPIRE].

[14] CMS collaboration, *The CMS Experiment at the CERN LHC*, 2008 *JINST* **3** S08004 [INSPIRE].

[15] CMS collaboration, *Particle-flow reconstruction and global event description with the CMS detector*, 2017 *JINST* **12** P10003 [arXiv:1706.04965] [INSPIRE].

[16] CMS collaboration, *Description and performance of track and primary-vertex reconstruction with the CMS tracker*, 2014 *JINST* **9** P10009 [arXiv:1405.6569] [INSPIRE].

[17] M. Cacciari, G.P. Salam and G. Soyez, *The anti-*k_t *jet clustering algorithm*, *JHEP* **04** (2008) 063 [arXiv:0802.1189] [INSPIRE].

[18] M. Cacciari, G.P. Salam and G. Soyez, *FastJet User Manual*, *Eur. Phys. J.* **C 72** (2012) 1896 [arXiv:1111.6097] [INSPIRE].

[19] CMS collaboration, *Jet energy scale and resolution in the CMS experiment in pp collisions at* 8 *TeV*, 2017 *JINST* **12** P02014 [arXiv:1607.03663] [INSPIRE].

[20] W. Adam, R. Frühwirth, A. Strandlie and T. Todorov, *Reconstruction of electrons with the Gaussian-sum filter in the CMS tracker at LHC*, *J. Phys.* **G 31** (2005) N9 [*eConf* **C 0303241** (2003) TULT009] [physics/0306087] [INSPIRE].

[21] CMS collaboration, *Performance of Electron Reconstruction and Selection with the CMS Detector in Proton-Proton Collisions at* $\sqrt{s} = 8$ *TeV*, 2015 *JINST* **10** P06005 [arXiv:1502.02701] [INSPIRE].

[22] CMS collaboration, *CMS Luminosity Measurements for the 2016 Data Taking Period*, CMS-PAS-LUM-17-001 (2017) [INSPIRE].

JHEP02(2019)074

[23] CMS collaboration, *Performance of Photon Reconstruction and Identification with the CMS Detector in Proton-Proton Collisions at* $\sqrt{s} = 8$ *TeV*, 2015 *JINST* **10** P08010 [arXiv:1502.02702] [INSPIRE].

[24] NNPDF collaboration, *Parton distributions for the LHC Run II*, *JHEP* **04** (2015) 040 [arXiv:1410.8849] [INSPIRE].

[25] NNPDF collaboration, *Parton distributions from high-precision collider data*, *Eur. Phys. J.* **C 77** (2017) 663 [arXiv:1706.00428] [INSPIRE].

[26] J. Alwall et al., *The automated computation of tree-level and next-to-leading order differential cross sections and their matching to parton shower simulations*, *JHEP* **07** (2014) 079 [arXiv:1405.0301] [INSPIRE].

[27] CMS collaboration, *Event generator tunes obtained from underlying event and multiparton scattering measurements*, *Eur. Phys. J.* **C 76** (2016) 155 [arXiv:1512.00815] [INSPIRE].

[28] GEANT4 collaboration, *GEANT4: A Simulation toolkit*, *Nucl. Instrum. Meth.* **A 506** (2003) 250 [INSPIRE].

[29] J. Allison et al., *Geant4 developments and applications*, *IEEE Trans. Nucl. Sci.* **53** (2006) 270 [INSPIRE].

[30] S. Catani, D. de Florian, G. Ferrera and M. Grazzini, *Vector boson production at hadron colliders: transverse-momentum resummation and leptonic decay*, *JHEP* **12** (2015) 047 [arXiv:1507.06937] [INSPIRE].

[31] A. Denner, S. Dittmaier, M. Hecht and C. Pasold, *NLO QCD and electroweak corrections to* $W + \gamma$ *production with leptonic W-boson decays*, *JHEP* **04** (2015) 018 [arXiv:1412.7421] [INSPIRE].

[32] A. Denner, S. Dittmaier, M. Hecht and C. Pasold, *NLO QCD and electroweak corrections to* $Z + \gamma$ *production with leptonic Z-boson decays*, *JHEP* **02** (2016) 057 [arXiv:1510.08742] [INSPIRE].

[33] A.V. Manohar, P. Nason, G.P. Salam and G. Zanderighi, *The Photon Content of the Proton*, *JHEP* **12** (2017) 046 [arXiv:1708.01256] [INSPIRE].

[34] J.M. Lindert et al., *Precise predictions for* V *+ jets dark matter backgrounds*, *Eur. Phys. J.* **C 77** (2017) 829 [arXiv:1705.04664] [INSPIRE].

[35] CMS collaboration, *Measurement of the Inclusive W and Z Production Cross Sections in pp Collisions at* $\sqrt{s} = 7$ *TeV*, *JHEP* **10** (2011) 132 [arXiv:1107.4789] [INSPIRE].

[36] CMS collaboration, *Search for Resonant Production of High-Mass Photon Pairs in Proton-Proton Collisions at* $\sqrt{s} = 8$ *and* 13 *TeV*, *Phys. Rev. Lett.* **117** (2016) 051802 [arXiv:1606.04093] [INSPIRE].

[37] CMS collaboration, *Simplified likelihood for the re-interpretation of public CMS results*, CMS-NOTE-2017-001 (2017).

[38] T. Junk, *Confidence level computation for combining searches with small statistics*, *Nucl. Instrum. Meth.* **A 434** (1999) 435 [hep-ex/9902006] [INSPIRE].

[39] A.L. Read, *Presentation of search results: The* CL_s *technique*, *J. Phys.* **G 28** (2002) 2693 [INSPIRE].

[40] G. Cowan, K. Cranmer, E. Gross and O. Vitells, *Asymptotic formulae for likelihood-based tests of new physics*, *Eur. Phys. J.* **C 71** (2011) 1554 [*Erratum ibid.* **C 73** (2013) 2501] [arXiv:1007.1727] [INSPIRE].

JHEP02(2019)074

[41] Planck collaboration, *Planck 2015 results. XIII. Cosmological parameters*, *Astron. Astrophys.* **594** (2016) A13 [arXiv:1502.01589] [inSPIRE].

[42] M. Backovic, K. Kong and M. McCaskey, *MadDM v.1.0: Computation of Dark Matter Relic Abundance Using MadGraph5*, *Phys. Dark Universe* **5–6** (2014) 18 [arXiv:1308.4955] [inSPIRE].

[43] SuperCDMS collaboration, *New Results from the Search for Low-Mass Weakly Interacting Massive Particles with the CDMS Low Ionization Threshold Experiment*, *Phys. Rev. Lett.* **116** (2016) 071301 [arXiv:1509.02448] [inSPIRE].

[44] LUX collaboration, *Results from a search for dark matter in the complete LUX exposure*, *Phys. Rev. Lett.* **118** (2017) 021303 [arXiv:1608.07648] [inSPIRE].

[45] PandaX-II collaboration, *Dark Matter Results From* 54*-Ton-Day Exposure of PandaX-II Experiment*, *Phys. Rev. Lett.* **119** (2017) 181302 [arXiv:1708.06917] [inSPIRE].

[46] XENON collaboration, *Dark Matter Search Results from a One Ton-Year Exposure of XENON1T*, *Phys. Rev. Lett.* **121** (2018) 111302 [arXiv:1805.12562] [inSPIRE].

[47] CRESST collaboration, *Results on light dark matter particles with a low-threshold CRESST-II detector*, *Eur. Phys. J.* **C 76** (2016) 25 [arXiv:1509.01515] [inSPIRE].

[48] PICO collaboration, *Dark Matter Search Results from the PICO-*60 C_3F_8 *Bubble Chamber*, *Phys. Rev. Lett.* **118** (2017) 251301 [arXiv:1702.07666] [inSPIRE].

[49] IceCube collaboration, *Improved limits on dark matter annihilation in the Sun with the* 79*-string IceCube detector and implications for supersymmetry*, *JCAP* **04** (2016) 022 [arXiv:1601.00653] [inSPIRE].

[50] E. Behnke et al., *Final Results of the PICASSO Dark Matter Search Experiment*, *Astropart. Phys.* **90** (2017) 85 [arXiv:1611.01499] [inSPIRE].

[51] Super-Kamiokande collaboration, *Search for neutrinos from annihilation of captured low-mass dark matter particles in the Sun by Super-Kamiokande*, *Phys. Rev. Lett.* **114** (2015) 141301 [arXiv:1503.04858] [inSPIRE].

JHEP02(2019)074

The CMS collaboration

Yerevan Physics Institute, Yerevan, Armenia

A.M. Sirunyan, A. Tumasyan

Institut für Hochenergiephysik, Wien, Austria

W. Adam, F. Ambrogi, E. Asilar, T. Bergauer, J. Brandstetter, M. Dragicevic, J. Erö, A. Escalante Del Valle, M. Flechl, R. Frühwirth[1], V.M. Ghete, J. Hrubec, M. Jeitler[1], N. Krammer, I. Krätschmer, D. Liko, T. Madlener, I. Mikulec, N. Rad, H. Rohringer, J. Schieck[1], R. Schöfbeck, M. Spanring, D. Spitzbart, A. Taurok, W. Waltenberger, J. Wittmann, C.-E. Wulz[1], M. Zarucki

Institute for Nuclear Problems, Minsk, Belarus

V. Chekhovsky, V. Mossolov, J. Suarez Gonzalez

Universiteit Antwerpen, Antwerpen, Belgium

E.A. De Wolf, D. Di Croce, X. Janssen, J. Lauwers, M. Pieters, H. Van Haevermaet, P. Van Mechelen, N. Van Remortel

Vrije Universiteit Brussel, Brussel, Belgium

S. Abu Zeid, F. Blekman, J. D'Hondt, J. De Clercq, K. Deroover, G. Flouris, D. Lontkovskyi, S. Lowette, I. Marchesini, S. Moortgat, L. Moreels, Q. Python, K. Skovpen, S. Tavernier, W. Van Doninck, P. Van Mulders, I. Van Parijs

Université Libre de Bruxelles, Bruxelles, Belgium

D. Beghin, B. Bilin, H. Brun, B. Clerbaux, G. De Lentdecker, H. Delannoy, B. Dorney, G. Fasanella, L. Favart, R. Goldouzian, A. Grebenyuk, A.K. Kalsi, T. Lenzi, J. Luetic, N. Postiau, E. Starling, L. Thomas, C. Vander Velde, P. Vanlaer, D. Vannerom, Q. Wang

Ghent University, Ghent, Belgium

T. Cornelis, D. Dobur, A. Fagot, M. Gul, I. Khvastunov[2], D. Poyraz, C. Roskas, D. Trocino, M. Tytgat, W. Verbeke, B. Vermassen, M. Vit, N. Zaganidis

Université Catholique de Louvain, Louvain-la-Neuve, Belgium

H. Bakhshiansohi, O. Bondu, S. Brochet, G. Bruno, C. Caputo, P. David, C. Delaere, M. Delcourt, A. Giammanco, G. Krintiras, V. Lemaitre, A. Magitteri, K. Piotrzkowski, A. Saggio, M. Vidal Marono, S. Wertz, J. Zobec

Centro Brasileiro de Pesquisas Fisicas, Rio de Janeiro, Brazil

F.L. Alves, G.A. Alves, M. Correa Martins Junior, G. Correia Silva, C. Hensel, A. Moraes, M.E. Pol, P. Rebello Teles

Universidade do Estado do Rio de Janeiro, Rio de Janeiro, Brazil

E. Belchior Batista Das Chagas, W. Carvalho, J. Chinellato[3], E. Coelho, E.M. Da Costa, G.G. Da Silveira[4], D. De Jesus Damiao, C. De Oliveira Martins, S. Fonseca De Souza, H. Malbouisson, D. Matos Figueiredo, M. Melo De Almeida, C. Mora Herrera, L. Mundim, H. Nogima, W.L. Prado Da Silva, L.J. Sanchez Rosas, A. Santoro, A. Sznajder, M. Thiel, E.J. Tonelli Manganote[3], F. Torres Da Silva De Araujo, A. Vilela Pereira

JHEP02(2019)074

Universidade Estadual Paulista [a], Universidade Federal do ABC [b], São Paulo, Brazil

S. Ahuja[a], C.A. Bernardes[a], L. Calligaris[a], T.R. Fernandez Perez Tomei[a], E.M. Gregores[b], P.G. Mercadante[b], S.F. Novaes[a], SandraS. Padula[a]

Institute for Nuclear Research and Nuclear Energy, Bulgarian Academy of Sciences, Sofia, Bulgaria

A. Aleksandrov, R. Hadjiiska, P. Iaydjiev, A. Marinov, M. Misheva, M. Rodozov, M. Shopova, G. Sultanov

University of Sofia, Sofia, Bulgaria

A. Dimitrov, L. Litov, B. Pavlov, P. Petkov

Beihang University, Beijing, China

W. Fang[5], X. Gao[5], L. Yuan

Institute of High Energy Physics, Beijing, China

M. Ahmad, J.G. Bian, G.M. Chen, H.S. Chen, M. Chen, Y. Chen, C.H. Jiang, D. Leggat, H. Liao, Z. Liu, F. Romeo, S.M. Shaheen[6], A. Spiezia, J. Tao, Z. Wang, E. Yazgan, H. Zhang, S. Zhang[6], J. Zhao

State Key Laboratory of Nuclear Physics and Technology, Peking University, Beijing, China

Y. Ban, G. Chen, A. Levin, J. Li, L. Li, Q. Li, Y. Mao, S.J. Qian, D. Wang

Tsinghua University, Beijing, China

Y. Wang

Universidad de Los Andes, Bogota, Colombia

C. Avila, A. Cabrera, C.A. Carrillo Montoya, L.F. Chaparro Sierra, C. Florez, C.F. González Hernández, M.A. Segura Delgado

University of Split, Faculty of Electrical Engineering, Mechanical Engineering and Naval Architecture, Split, Croatia

B. Courbon, N. Godinovic, D. Lelas, I. Puljak, T. Sculac

University of Split, Faculty of Science, Split, Croatia

Z. Antunovic, M. Kovac

Institute Rudjer Boskovic, Zagreb, Croatia

V. Brigljevic, D. Ferencek, K. Kadija, B. Mesic, A. Starodumov[7], T. Susa

University of Cyprus, Nicosia, Cyprus

M.W. Ather, A. Attikis, M. Kolosova, G. Mavromanolakis, J. Mousa, C. Nicolaou, F. Ptochos, P.A. Razis, H. Rykaczewski

Charles University, Prague, Czech Republic

M. Finger[8], M. Finger Jr.[8]

JHEP02(2019)074

Escuela Politecnica Nacional, Quito, Ecuador

E. Ayala

Universidad San Francisco de Quito, Quito, Ecuador

E. Carrera Jarrin

Academy of Scientific Research and Technology of the Arab Republic of Egypt, Egyptian Network of High Energy Physics, Cairo, Egypt

Y. Assran[9,10], S. Elgammal[10], A. Ellithi Kamel[11]

National Institute of Chemical Physics and Biophysics, Tallinn, Estonia

S. Bhowmik, A. Carvalho Antunes De Oliveira, R.K. Dewanjee, K. Ehataht, M. Kadastik, M. Raidal, C. Veelken

Department of Physics, University of Helsinki, Helsinki, Finland

P. Eerola, H. Kirschenmann, J. Pekkanen, M. Voutilainen

Helsinki Institute of Physics, Helsinki, Finland

J. Havukainen, J.K. Heikkilä, T. Järvinen, V. Karimäki, R. Kinnunen, T. Lampén, K. Lassila-Perini, S. Laurila, S. Lehti, T. Lindén, P. Luukka, T. Mäenpää, H. Siikonen, E. Tuominen, J. Tuominiemi

Lappeenranta University of Technology, Lappeenranta, Finland

T. Tuuva

IRFU, CEA, Université Paris-Saclay, Gif-sur-Yvette, France

M. Besancon, F. Couderc, M. Dejardin, D. Denegri, J.L. Faure, F. Ferri, S. Ganjour, A. Givernaud, P. Gras, G. Hamel de Monchenault, P. Jarry, C. Leloup, E. Locci, J. Malcles, G. Negro, J. Rander, A. Rosowsky, M.Ö. Sahin, M. Titov

Laboratoire Leprince-Ringuet, Ecole polytechnique, CNRS/IN2P3, Université Paris-Saclay, Palaiseau, France

A. Abdulsalam[12], C. Amendola, I. Antropov, F. Beaudette, P. Busson, C. Charlot, R. Granier de Cassagnac, I. Kucher, A. Lobanov, J. Martin Blanco, C. Martin Perez, M. Nguyen, C. Ochando, G. Ortona, P. Paganini, P. Pigard, J. Rembser, R. Salerno, J.B. Sauvan, Y. Sirois, A.G. Stahl Leiton, A. Zabi, A. Zghiche

Université de Strasbourg, CNRS, IPHC UMR 7178, Strasbourg, France

J.-L. Agram[13], J. Andrea, D. Bloch, J.-M. Brom, E.C. Chabert, V. Cherepanov, C. Collard, E. Conte[13], J.-C. Fontaine[13], D. Gelé, U. Goerlach, M. Jansová, A.-C. Le Bihan, N. Tonon, P. Van Hove

Centre de Calcul de l'Institut National de Physique Nucleaire et de Physique des Particules, CNRS/IN2P3, Villeurbanne, France

S. Gadrat

JHEP02(2019)074

Université de Lyon, Université Claude Bernard Lyon 1, CNRS-IN2P3, Institut de Physique Nucléaire de Lyon, Villeurbanne, France
S. Beauceron, C. Bernet, G. Boudoul, N. Chanon, R. Chierici, D. Contardo, P. Depasse, H. El Mamouni, J. Fay, L. Finco, S. Gascon, M. Gouzevitch, G. Grenier, B. Ille, F. Lagarde, I.B. Laktineh, H. Lattaud, M. Lethuillier, L. Mirabito, S. Perries, A. Popov[14], V. Sordini, G. Touquet, M. Vander Donckt, S. Viret

Georgian Technical University, Tbilisi, Georgia
T. Toriashvili[15]

Tbilisi State University, Tbilisi, Georgia
I. Bagaturia[16]

RWTH Aachen University, I. Physikalisches Institut, Aachen, Germany
C. Autermann, L. Feld, M.K. Kiesel, K. Klein, M. Lipinski, M. Preuten, M.P. Rauch, C. Schomakers, J. Schulz, M. Teroerde, B. Wittmer

RWTH Aachen University, III. Physikalisches Institut A, Aachen, Germany
A. Albert, D. Duchardt, M. Erdmann, S. Erdweg, T. Esch, R. Fischer, S. Ghosh, A. Güth, T. Hebbeker, C. Heidemann, K. Hoepfner, H. Keller, L. Mastrolorenzo, M. Merschmeyer, A. Meyer, P. Millet, S. Mukherjee, T. Pook, M. Radziej, H. Reithler, M. Rieger, A. Schmidt, D. Teyssier, S. Thüer

RWTH Aachen University, III. Physikalisches Institut B, Aachen, Germany
G. Flügge, O. Hlushchenko, T. Kress, T. Müller, A. Nehrkorn, A. Nowack, C. Pistone, O. Pooth, D. Roy, H. Sert, A. Stahl[17]

Deutsches Elektronen-Synchrotron, Hamburg, Germany
M. Aldaya Martin, T. Arndt, C. Asawatangtrakuldee, I. Babounikau, K. Beernaert, O. Behnke, U. Behrens, A. Bermúdez Martínez, D. Bertsche, A.A. Bin Anuar, K. Borras[18], V. Botta, A. Campbell, P. Connor, C. Contreras-Campana, V. Danilov, A. De Wit, M.M. Defranchis, C. Diez Pardos, D. Domínguez Damiani, G. Eckerlin, T. Eichhorn, A. Elwood, E. Eren, E. Gallo[19], A. Geiser, J.M. Grados Luyando, A. Grohsjean, M. Guthoff, M. Haranko, A. Harb, J. Hauk, H. Jung, M. Kasemann, J. Keaveney, C. Kleinwort, J. Knolle, D. Krücker, W. Lange, A. Lelek, T. Lenz, J. Leonard, K. Lipka, W. Lohmann[20], R. Mankel, I.-A. Melzer-Pellmann, A.B. Meyer, M. Meyer, M. Missiroli, G. Mittag, J. Mnich, V. Myronenko, S.K. Pflitsch, D. Pitzl, A. Raspereza, M. Savitskyi, P. Saxena, P. Schütze, C. Schwanenberger, R. Shevchenko, A. Singh, H. Tholen, O. Turkot, A. Vagnerini, G.P. Van Onsem, R. Walsh, Y. Wen, K. Wichmann, C. Wissing, O. Zenaiev

University of Hamburg, Hamburg, Germany
R. Aggleton, S. Bein, L. Benato, A. Benecke, V. Blobel, T. Dreyer, A. Ebrahimi, E. Garutti, D. Gonzalez, P. Gunnellini, J. Haller, A. Hinzmann, A. Karavdina, G. Kasieczka, R. Klanner, R. Kogler, N. Kovalchuk, S. Kurz, V. Kutzner, J. Lange, D. Marconi, J. Multhaup, M. Niedziela, C.E.N. Niemeyer, D. Nowatschin, A. Perieanu, A. Reimers, O. Rieger, C. Scharf, P. Schleper, S. Schumann, J. Schwandt, J. Sonneveld, H. Stadie, G. Steinbrück, F.M. Stober, M. Stöver, A. Vanhoefer, B. Vormwald, I. Zoi

JHEP02(2019)074

Karlsruher Institut fuer Technologie, Karlsruhe, Germany
M. Akbiyik, C. Barth, M. Baselga, S. Baur, E. Butz, R. Caspart, T. Chwalek, F. Colombo, W. De Boer, A. Dierlamm, K. El Morabit, N. Faltermann, B. Freund, M. Giffels, M.A. Harrendorf, F. Hartmann[17], S.M. Heindl, U. Husemann, I. Katkov[14], S. Kudella, S. Mitra, M.U. Mozer, Th. Müller, M. Musich, M. Plagge, G. Quast, K. Rabbertz, M. Schröder, I. Shvetsov, H.J. Simonis, R. Ulrich, S. Wayand, M. Weber, T. Weiler, C. Wöhrmann, R. Wolf

Institute of Nuclear and Particle Physics (INPP), NCSR Demokritos, Aghia Paraskevi, Greece
G. Anagnostou, G. Daskalakis, T. Geralis, A. Kyriakis, D. Loukas, G. Paspalaki

National and Kapodistrian University of Athens, Athens, Greece
G. Karathanasis, P. Kontaxakis, A. Panagiotou, I. Papavergou, N. Saoulidou, E. Tziaferi, K. Vellidis

National Technical University of Athens, Athens, Greece
K. Kousouris, I. Papakrivopoulos, G. Tsipolitis

University of Ioánnina, Ioánnina, Greece
I. Evangelou, C. Foudas, P. Gianneios, P. Katsoulis, P. Kokkas, S. Mallios, N. Manthos, I. Papadopoulos, E. Paradas, J. Strologas, F.A. Triantis, D. Tsitsonis

MTA-ELTE Lendület CMS Particle and Nuclear Physics Group, Eötvös Loránd University, Budapest, Hungary
M. Bartók[21], M. Csanad, N. Filipovic, P. Major, M.I. Nagy, G. Pasztor, O. Surányi, G.I. Veres

Wigner Research Centre for Physics, Budapest, Hungary
G. Bencze, C. Hajdu, D. Horvath[22], Á. Hunyadi, F. Sikler, T.Á. Vámi, V. Veszpremi, G. Vesztergombi[†]

Institute of Nuclear Research ATOMKI, Debrecen, Hungary
N. Beni, S. Czellar, J. Karancsi[21], A. Makovec, J. Molnar, Z. Szillasi

Institute of Physics, University of Debrecen, Debrecen, Hungary
P. Raics, Z.L. Trocsanyi, B. Ujvari

Indian Institute of Science (IISc), Bangalore, India
S. Choudhury, J.R. Komaragiri, P.C. Tiwari

National Institute of Science Education and Research, HBNI, Bhubaneswar, India
S. Bahinipati[24], C. Kar, P. Mal, K. Mandal, A. Nayak[25], D.K. Sahoo[24], S.K. Swain

Panjab University, Chandigarh, India
S. Bansal, S.B. Beri, V. Bhatnagar, S. Chauhan, R. Chawla, N. Dhingra, R. Gupta, A. Kaur, M. Kaur, S. Kaur, P. Kumari, M. Lohan, A. Mehta, K. Sandeep, S. Sharma, J.B. Singh, A.K. Virdi, G. Walia

JHEP02(2019)074

University of Delhi, Delhi, India

A. Bhardwaj, B.C. Choudhary, R.B. Garg, M. Gola, S. Keshri, Ashok Kumar, S. Malhotra, M. Naimuddin, P. Priyanka, K. Ranjan, Aashaq Shah, R. Sharma

Saha Institute of Nuclear Physics, HBNI, Kolkata, India

R. Bhardwaj[26], M. Bharti[26], R. Bhattacharya, S. Bhattacharya, U. Bhawandeep[26], D. Bhowmik, S. Dey, S. Dutt[26], S. Dutta, S. Ghosh, K. Mondal, S. Nandan, A. Purohit, P.K. Rout, A. Roy, S. Roy Chowdhury, G. Saha, S. Sarkar, M. Sharan, B. Singh[26], S. Thakur[26]

Indian Institute of Technology Madras, Madras, India

P.K. Behera

Bhabha Atomic Research Centre, Mumbai, India

R. Chudasama, D. Dutta, V. Jha, V. Kumar, P.K. Netrakanti, L.M. Pant, P. Shukla

Tata Institute of Fundamental Research-A, Mumbai, India

T. Aziz, M.A. Bhat, S. Dugad, G.B. Mohanty, N. Sur, B. Sutar, RavindraKumar Verma

Tata Institute of Fundamental Research-B, Mumbai, India

S. Banerjee, S. Bhattacharya, S. Chatterjee, P. Das, M. Guchait, Sa. Jain, S. Karmakar, S. Kumar, M. Maity[27], G. Majumder, K. Mazumdar, N. Sahoo, T. Sarkar[27]

Indian Institute of Science Education and Research (IISER), Pune, India

S. Chauhan, S. Dube, V. Hegde, A. Kapoor, K. Kothekar, S. Pandey, A. Rane, A. Rastogi, S. Sharma

Institute for Research in Fundamental Sciences (IPM), Tehran, Iran

S. Chenarani[28], E. Eskandari Tadavani, S.M. Etesami[28], M. Khakzad, M. Mohammadi Najafabadi, M. Naseri, F. Rezaei Hosseinabadi, B. Safarzadeh[29], M. Zeinali

University College Dublin, Dublin, Ireland

M. Felcini, M. Grunewald

INFN Sezione di Bari [a], Università di Bari [b], Politecnico di Bari [c], Bari, Italy

M. Abbrescia[a,b], C. Calabria[a,b], A. Colaleo[a], D. Creanza[a,c], L. Cristella[a,b], N. De Filippis[a,c], M. De Palma[a,b], A. Di Florio[a,b], F. Errico[a,b], L. Fiore[a], A. Gelmi[a,b], G. Iaselli[a,c], M. Ince[a,b], S. Lezki[a,b], G. Maggi[a,c], M. Maggi[a], G. Miniello[a,b], S. My[a,b], S. Nuzzo[a,b], A. Pompili[a,b], G. Pugliese[a,c], R. Radogna[a], A. Ranieri[a], G. Selvaggi[a,b], A. Sharma[a], L. Silvestris[a], R. Venditti[a], P. Verwilligen[a], G. Zito[a]

INFN Sezione di Bologna [a], Università di Bologna [b], Bologna, Italy

G. Abbiendi[a], C. Battilana[a,b], D. Bonacorsi[a,b], L. Borgonovi[a,b], S. Braibant-Giacomelli[a,b], R. Campanini[a,b], P. Capiluppi[a,b], A. Castro[a,b], F.R. Cavallo[a], S.S. Chhibra[a,b], C. Ciocca[a], G. Codispoti[a,b], M. Cuffiani[a,b], G.M. Dallavalle[a], F. Fabbri[a], A. Fanfani[a,b], E. Fontanesi, P. Giacomelli[a], C. Grandi[a], L. Guiducci[a,b], S. Lo Meo[a], S. Marcellini[a], G. Masetti[a], A. Montanari[a], F.L. Navarria[a,b], A. Perrotta[a], F. Primavera[a,b,17], A.M. Rossi[a,b], T. Rovelli[a,b], G.P. Siroli[a,b], N. Tosi[a]

JHEP02(2019)074

INFN Sezione di Catania [a], Università di Catania [b], Catania, Italy

S. Albergo[a,b], A. Di Mattia[a], R. Potenza[a,b], A. Tricomi[a,b], C. Tuve[a,b]

INFN Sezione di Firenze [a], Università di Firenze [b], Firenze, Italy

G. Barbagli[a], K. Chatterjee[a,b], V. Ciulli[a,b], C. Civinini[a], R. D'Alessandro[a,b], E. Focardi[a,b], G. Latino, P. Lenzi[a,b], M. Meschini[a], S. Paoletti[a], L. Russo[a,30], G. Sguazzoni[a], D. Strom[a], L. Viliani[a]

INFN Laboratori Nazionali di Frascati, Frascati, Italy

L. Benussi, S. Bianco, F. Fabbri, D. Piccolo

INFN Sezione di Genova [a], Università di Genova [b], Genova, Italy

F. Ferro[a], R. Mulargia[a,b], F. Ravera[a,b], E. Robutti[a], S. Tosi[a,b]

INFN Sezione di Milano-Bicocca [a], Università di Milano-Bicocca [b], Milano, Italy

A. Benaglia[a], A. Beschi[b], F. Brivio[a,b], V. Ciriolo[a,b,17], S. Di Guida[a,d,17], M.E. Dinardo[a,b], S. Fiorendi[a,b], S. Gennai[a], A. Ghezzi[a,b], P. Govoni[a,b], M. Malberti[a,b], S. Malvezzi[a], D. Menasce[a], F. Monti, L. Moroni[a], M. Paganoni[a,b], D. Pedrini[a], S. Ragazzi[a,b], T. Tabarelli de Fatis[a,b], D. Zuolo[a,b]

INFN Sezione di Napoli [a], Università di Napoli 'Federico II' [b], Napoli, Italy, Università della Basilicata [c], Potenza, Italy, Università G. Marconi [d], Roma, Italy

S. Buontempo[a], N. Cavallo[a,c], A. De Iorio[a,b], A. Di Crescenzo[a,b], F. Fabozzi[a,c], F. Fienga[a], G. Galati[a], A.O.M. Iorio[a,b], W.A. Khan[a], L. Lista[a], S. Meola[a,d,17], P. Paolucci[a,17], C. Sciacca[a,b], E. Voevodina[a,b]

INFN Sezione di Padova [a], Università di Padova [b], Padova, Italy, Università di Trento [c], Trento, Italy

P. Azzi[a], N. Bacchetta[a], D. Bisello[a,b], A. Boletti[a,b], A. Bragagnolo, R. Carlin[a,b], P. Checchia[a], M. Dall'Osso[a,b], P. De Castro Manzano[a], T. Dorigo[a], U. Dosselli[a], F. Gasparini[a,b], U. Gasparini[a,b], A. Gozzelino[a], S.Y. Hoh, S. Lacaprara[a], P. Lujan, M. Margoni[a,b], A.T. Meneguzzo[a,b], J. Pazzini[a,b], P. Ronchese[a,b], R. Rossin[a,b], F. Simonetto[a,b], A. Tiko, E. Torassa[a], M. Tosi[a,b], M. Zanetti[a,b], P. Zotto[a,b], G. Zumerle[a,b]

INFN Sezione di Pavia [a], Università di Pavia [b], Pavia, Italy

A. Braghieri[a], A. Magnani[a], P. Montagna[a,b], S.P. Ratti[a,b], V. Re[a], M. Ressegotti[a,b], C. Riccardi[a,b], P. Salvini[a], I. Vai[a,b], P. Vitulo[a,b]

INFN Sezione di Perugia [a], Università di Perugia [b], Perugia, Italy

M. Biasini[a,b], G.M. Bilei[a], C. Cecchi[a,b], D. Ciangottini[a,b], L. Fanò[a,b], P. Lariccia[a,b], R. Leonardi[a,b], E. Manoni[a], G. Mantovani[a,b], V. Mariani[a,b], M. Menichelli[a], A. Rossi[a,b], A. Santocchia[a,b], D. Spiga[a]

JHEP02(2019)074

INFN Sezione di Pisa [a], Università di Pisa [b], Scuola Normale Superiore di Pisa [c], Pisa, Italy

K. Androsov[a], P. Azzurri[a], G. Bagliesi[a], L. Bianchini[a], T. Boccali[a], L. Borrello, R. Castaldi[a], M.A. Ciocci[a,b], R. Dell'Orso[a], G. Fedi[a], F. Fiori[a,c], L. Giannini[a,c], A. Giassi[a], M.T. Grippo[a], F. Ligabue[a,c], E. Manca[a,c], G. Mandorli[a,c], A. Messineo[a,b], F. Palla[a], A. Rizzi[a,b], G. Rolandi[31], P. Spagnolo[a], R. Tenchini[a], G. Tonelli[a,b], A. Venturi[a], P.G. Verdini[a]

INFN Sezione di Roma [a], Sapienza Università di Roma [b], Rome, Italy

L. Barone[a,b], F. Cavallari[a], M. Cipriani[a,b], D. Del Re[a,b], E. Di Marco[a,b], M. Diemoz[a], S. Gelli[a,b], E. Longo[a,b], B. Marzocchi[a,b], P. Meridiani[a], G. Organtini[a,b], F. Pandolfi[a], R. Paramatti[a,b], F. Preiato[a,b], S. Rahatlou[a,b], C. Rovelli[a], F. Santanastasio[a,b]

INFN Sezione di Torino [a], Università di Torino [b], Torino, Italy, Università del Piemonte Orientale [c], Novara, Italy

N. Amapane[a,b], R. Arcidiacono[a,c], S. Argiro[a,b], M. Arneodo[a,c], N. Bartosik[a], R. Bellan[a,b], C. Biino[a], A. Cappati[a,b], N. Cartiglia[a], F. Cenna[a,b], S. Cometti[a], M. Costa[a,b], R. Covarelli[a,b], N. Demaria[a], B. Kiani[a,b], C. Mariotti[a], S. Maselli[a], E. Migliore[a,b], V. Monaco[a,b], E. Monteil[a,b], M. Monteno[a], M.M. Obertino[a,b], L. Pacher[a,b], N. Pastrone[a], M. Pelliccioni[a], G.L. Pinna Angioni[a,b], A. Romero[a,b], M. Ruspa[a,c], R. Sacchi[a,b], R. Salvatico[a,b], K. Shchelina[a,b], V. Sola[a], A. Solano[a,b], D. Soldi[a,b], A. Staiano[a]

INFN Sezione di Trieste [a], Università di Trieste [b], Trieste, Italy

S. Belforte[a], V. Candelise[a,b], M. Casarsa[a], F. Cossutti[a], A. Da Rold[a,b], G. Della Ricca[a,b], F. Vazzoler[a,b], A. Zanetti[a]

Kyungpook National University, Daegu, Korea

D.H. Kim, G.N. Kim, M.S. Kim, J. Lee, S. Lee, S.W. Lee, C.S. Moon, Y.D. Oh, S.I. Pak, S. Sekmen, D.C. Son, Y.C. Yang

Chonnam National University, Institute for Universe and Elementary Particles, Kwangju, Korea

H. Kim, D.H. Moon, G. Oh

Hanyang University, Seoul, Korea

B. Francois, J. Goh[32], T.J. Kim

Korea University, Seoul, Korea

S. Cho, S. Choi, Y. Go, D. Gyun, S. Ha, B. Hong, Y. Jo, K. Lee, K.S. Lee, S. Lee, J. Lim, S.K. Park, Y. Roh

Sejong University, Seoul, Korea

H.S. Kim

Seoul National University, Seoul, Korea

J. Almond, J. Kim, J.S. Kim, H. Lee, K. Lee, K. Nam, S.B. Oh, B.C. Radburn-Smith, S.h. Seo, U.K. Yang, H.D. Yoo, G.B. Yu

JHEP02(2019)074

University of Seoul, Seoul, Korea
D. Jeon, H. Kim, J.H. Kim, J.S.H. Lee, I.C. Park

Sungkyunkwan University, Suwon, Korea
Y. Choi, C. Hwang, J. Lee, I. Yu

Vilnius University, Vilnius, Lithuania
V. Dudenas, A. Juodagalvis, J. Vaitkus

National Centre for Particle Physics, Universiti Malaya, Kuala Lumpur, Malaysia
I. Ahmed, Z.A. Ibrahim, M.A.B. Md Ali[33], F. Mohamad Idris[34], W.A.T. Wan Abdullah, M.N. Yusli, Z. Zolkapli

Universidad de Sonora (UNISON), Hermosillo, Mexico
J.F. Benitez, A. Castaneda Hernandez, J.A. Murillo Quijada

Centro de Investigacion y de Estudios Avanzados del IPN, Mexico City, Mexico
H. Castilla-Valdez, E. De La Cruz-Burelo, M.C. Duran-Osuna, I. Heredia-De La Cruz[35], R. Lopez-Fernandez, J. Mejia Guisao, R.I. Rabadan-Trejo, M. Ramirez-Garcia, G. Ramirez-Sanchez, R. Reyes-Almanza, A. Sanchez-Hernandez

Universidad Iberoamericana, Mexico City, Mexico
S. Carrillo Moreno, C. Oropeza Barrera, F. Vazquez Valencia

Benemerita Universidad Autonoma de Puebla, Puebla, Mexico
J. Eysermans, I. Pedraza, H.A. Salazar Ibarguen, C. Uribe Estrada

Universidad Autónoma de San Luis Potosí, San Luis Potosí, Mexico
A. Morelos Pineda

University of Auckland, Auckland, New Zealand
D. Krofcheck

University of Canterbury, Christchurch, New Zealand
S. Bheesette, P.H. Butler

National Centre for Physics, Quaid-I-Azam University, Islamabad, Pakistan
A. Ahmad, M. Ahmad, M.I. Asghar, Q. Hassan, H.R. Hoorani, A. Saddique, M.A. Shah, M. Shoaib, M. Waqas

National Centre for Nuclear Research, Swierk, Poland
H. Bialkowska, M. Bluj, B. Boimska, T. Frueboes, M. Górski, M. Kazana, M. Szleper, P. Traczyk, P. Zalewski

Institute of Experimental Physics, Faculty of Physics, University of Warsaw, Warsaw, Poland
K. Bunkowski, A. Byszuk[36], K. Doroba, A. Kalinowski, M. Konecki, J. Krolikowski, M. Misiura, M. Olszewski, A. Pyskir, M. Walczak

JHEP02(2019)074

Laboratório de Instrumentação e Física Experimental de Partículas, Lisboa, Portugal

M. Araujo, P. Bargassa, C. Beirão Da Cruz E Silva, A. Di Francesco, P. Faccioli, B. Galinhas, M. Gallinaro, J. Hollar, N. Leonardo, J. Seixas, G. Strong, O. Toldaiev, J. Varela

Joint Institute for Nuclear Research, Dubna, Russia

S. Afanasiev, P. Bunin, M. Gavrilenko, I. Golutvin, I. Gorbunov, A. Kamenev, V. Karjavine, A. Lanev, A. Malakhov, V. Matveev[37,38], P. Moisenz, V. Palichik, V. Perelygin, S. Shmatov, S. Shulha, N. Skatchkov, V. Smirnov, N. Voytishin, A. Zarubin

Petersburg Nuclear Physics Institute, Gatchina (St. Petersburg), Russia

V. Golovtsov, Y. Ivanov, V. Kim[39], E. Kuznetsova[40], P. Levchenko, V. Murzin, V. Oreshkin, I. Smirnov, D. Sosnov, V. Sulimov, L. Uvarov, S. Vavilov, A. Vorobyev

Institute for Nuclear Research, Moscow, Russia

Yu. Andreev, A. Dermenev, S. Gninenko, N. Golubev, A. Karneyeu, M. Kirsanov, N. Krasnikov, A. Pashenkov, D. Tlisov, A. Toropin

Institute for Theoretical and Experimental Physics, Moscow, Russia

V. Epshteyn, V. Gavrilov, N. Lychkovskaya, V. Popov, I. Pozdnyakov, G. Safronov, A. Spiridonov, A. Stepennov, V. Stolin, M. Toms, E. Vlasov, A. Zhokin

Moscow Institute of Physics and Technology, Moscow, Russia

T. Aushev

National Research Nuclear University 'Moscow Engineering Physics Institute' (MEPhI), Moscow, Russia

R. Chistov[41], M. Danilov[41], P. Parygin, D. Philippov, S. Polikarpov[41], E. Tarkovskii

P.N. Lebedev Physical Institute, Moscow, Russia

V. Andreev, M. Azarkin, I. Dremin[38], M. Kirakosyan, A. Terkulov

Skobeltsyn Institute of Nuclear Physics, Lomonosov Moscow State University, Moscow, Russia

A. Baskakov, A. Belyaev, E. Boos, V. Bunichev, M. Dubinin[42], L. Dudko, A. Ershov, A. Gribushin, V. Klyukhin, O. Kodolova, I. Lokhtin, I. Miagkov, S. Obraztsov, V. Savrin, A. Snigirev

Novosibirsk State University (NSU), Novosibirsk, Russia

A. Barnyakov[43], V. Blinov[43], T. Dimova[43], L. Kardapoltsev[43], Y. Skovpen[43]

Institute for High Energy Physics of National Research Centre 'Kurchatov Institute', Protvino, Russia

I. Azhgirey, I. Bayshev, S. Bitioukov, D. Elumakhov, A. Godizov, V. Kachanov, A. Kalinin, D. Konstantinov, P. Mandrik, V. Petrov, R. Ryutin, S. Slabospitskii, A. Sobol, S. Troshin, N. Tyurin, A. Uzunian, A. Volkov

JHEP02(2019)074

National Research Tomsk Polytechnic University, Tomsk, Russia
A. Babaev, S. Baidali, V. Okhotnikov

University of Belgrade, Faculty of Physics and Vinca Institute of Nuclear Sciences, Belgrade, Serbia
P. Adzic[44], P. Cirkovic, D. Devetak, M. Dordevic, J. Milosevic

Centro de Investigaciones Energéticas Medioambientales y Tecnológicas (CIEMAT), Madrid, Spain
J. Alcaraz Maestre, A. Álvarez Fernández, I. Bachiller, M. Barrio Luna, J.A. Brochero Cifuentes, M. Cerrada, N. Colino, B. De La Cruz, A. Delgado Peris, C. Fernandez Bedoya, J.P. Fernández Ramos, J. Flix, M.C. Fouz, O. Gonzalez Lopez, S. Goy Lopez, J.M. Hernandez, M.I. Josa, D. Moran, A. Pérez-Calero Yzquierdo, J. Puerta Pelayo, I. Redondo, L. Romero, M.S. Soares, A. Triossi

Universidad Autónoma de Madrid, Madrid, Spain
C. Albajar, J.F. de Trocóniz

Universidad de Oviedo, Oviedo, Spain
J. Cuevas, C. Erice, J. Fernandez Menendez, S. Folgueras, I. Gonzalez Caballero, J.R. González Fernández, E. Palencia Cortezon, V. Rodríguez Bouza, S. Sanchez Cruz, P. Vischia, J.M. Vizan Garcia

Instituto de Física de Cantabria (IFCA), CSIC-Universidad de Cantabria, Santander, Spain
I.J. Cabrillo, A. Calderon, B. Chazin Quero, J. Duarte Campderros, M. Fernandez, P.J. Fernández Manteca, A. García Alonso, J. Garcia-Ferrero, G. Gomez, A. Lopez Virto, J. Marco, C. Martinez Rivero, P. Martinez Ruiz del Arbol, F. Matorras, J. Piedra Gomez, C. Prieels, T. Rodrigo, A. Ruiz-Jimeno, L. Scodellaro, N. Trevisani, I. Vila, R. Vilar Cortabitarte

University of Ruhuna, Department of Physics, Matara, Sri Lanka
N. Wickramage

CERN, European Organization for Nuclear Research, Geneva, Switzerland
D. Abbaneo, B. Akgun, E. Auffray, G. Auzinger, P. Baillon, A.H. Ball, D. Barney, J. Bendavid, M. Bianco, A. Bocci, C. Botta, E. Brondolin, T. Camporesi, M. Cepeda, G. Cerminara, E. Chapon, Y. Chen, G. Cucciati, D. d'Enterria, A. Dabrowski, N. Daci, V. Daponte, A. David, A. De Roeck, N. Deelen, M. Dobson, M. Dünser, N. Dupont, A. Elliott-Peisert, P. Everaerts, F. Fallavollita[45], D. Fasanella, G. Franzoni, J. Fulcher, W. Funk, D. Gigi, A. Gilbert, K. Gill, F. Glege, M. Gruchala, M. Guilbaud, D. Gulhan, J. Hegeman, C. Heidegger, V. Innocente, A. Jafari, P. Janot, O. Karacheban[20], J. Kieseler, A. Kornmayer, M. Krammer[1], C. Lange, P. Lecoq, C. Lourenço, L. Malgeri, M. Mannelli, A. Massironi, F. Meijers, J.A. Merlin, S. Mersi, E. Meschi, P. Milenovic[46], F. Moortgat, M. Mulders, J. Ngadiuba, S. Nourbakhsh, S. Orfanelli, L. Orsini, F. Pantaleo[17], L. Pape, E. Perez, M. Peruzzi, A. Petrilli, G. Petrucciani, A. Pfeiffer, M. Pierini, F.M. Pitters, D. Rabady, A. Racz, T. Reis, M. Rovere, H. Sakulin, C. Schäfer, C. Schwick, M. Selvaggi,

JHEP02(2019)074

A. Sharma, P. Silva, P. Sphicas[47], A. Stakia, J. Steggemann, D. Treille, A. Tsirou, V. Veckalns[48], M. Verzetti, W.D. Zeuner

Paul Scherrer Institut, Villigen, Switzerland

L. Caminada[49], K. Deiters, W. Erdmann, R. Horisberger, Q. Ingram, H.C. Kaestli, D. Kotlinski, U. Langenegger, T. Rohe, S.A. Wiederkehr

ETH Zurich — Institute for Particle Physics and Astrophysics (IPA), Zurich, Switzerland

M. Backhaus, L. Bäni, P. Berger, N. Chernyavskaya, G. Dissertori, M. Dittmar, M. Donegà, C. Dorfer, T.A. Gómez Espinosa, C. Grab, D. Hits, T. Klijnsma, W. Lustermann, R.A. Manzoni, M. Marionneau, M.T. Meinhard, F. Micheli, P. Musella, F. Nessi-Tedaldi, J. Pata, F. Pauss, G. Perrin, L. Perrozzi, S. Pigazzini, M. Quittnat, C. Reissel, D. Ruini, D.A. Sanz Becerra, M. Schönenberger, L. Shchutska, V.R. Tavolaro, K. Theofilatos, M.L. Vesterbacka Olsson, R. Wallny, D.H. Zhu

Universität Zürich, Zurich, Switzerland

T.K. Aarrestad, C. Amsler[50], D. Brzhechko, M.F. Canelli, A. De Cosa, R. Del Burgo, S. Donato, C. Galloni, T. Hreus, B. Kilminster, S. Leontsinis, I. Neutelings, G. Rauco, P. Robmann, D. Salerno, K. Schweiger, C. Seitz, Y. Takahashi, A. Zucchetta

National Central University, Chung-Li, Taiwan

T.H. Doan, R. Khurana, C.M. Kuo, W. Lin, A. Pozdnyakov, S.S. Yu

National Taiwan University (NTU), Taipei, Taiwan

P. Chang, Y. Chao, K.F. Chen, P.H. Chen, W.-S. Hou, Arun Kumar, Y.F. Liu, R.-S. Lu, E. Paganis, A. Psallidas, A. Steen

Chulalongkorn University, Faculty of Science, Department of Physics, Bangkok, Thailand

B. Asavapibhop, N. Srimanobhas, N. Suwonjandee

Çukurova University, Physics Department, Science and Art Faculty, Adana, Turkey

A. Bat, F. Boran, S. Cerci[51], S. Damarseckin, Z.S. Demiroglu, F. Dolek, C. Dozen, I. Dumanoglu, E. Eskut, S. Girgis, G. Gokbulut, Y. Guler, E. Gurpinar, I. Hos[52], C. Isik, E.E. Kangal[53], O. Kara, A. Kayis Topaksu, U. Kiminsu, M. Oglakci, G. Onengut, K. Ozdemir[54], A. Polatoz, B. Tali[51], U.G. Tok, S. Turkcapar, I.S. Zorbakir, C. Zorbilmez

Middle East Technical University, Physics Department, Ankara, Turkey

B. Isildak[55], G. Karapinar[56], M. Yalvac, M. Zeyrek

Bogazici University, Istanbul, Turkey

I.O. Atakisi, E. Gülmez, M. Kaya[57], O. Kaya[58], S. Ozkorucuklu[59], S. Tekten, E.A. Yetkin[60]

Istanbul Technical University, Istanbul, Turkey

M.N. Agaras, A. Cakir, K. Cankocak, Y. Komurcu, S. Sen[61]

JHEP02(2019)074

Institute for Scintillation Materials of National Academy of Science of Ukraine, Kharkov, Ukraine

B. Grynyov

National Scientific Center, Kharkov Institute of Physics and Technology, Kharkov, Ukraine

L. Levchuk

University of Bristol, Bristol, United Kingdom

F. Ball, J.J. Brooke, D. Burns, E. Clement, D. Cussans, O. Davignon, H. Flacher, J. Goldstein, G.P. Heath, H.F. Heath, L. Kreczko, D.M. Newbold[62], S. Paramesvaran, B. Penning, T. Sakuma, D. Smith, V.J. Smith, J. Taylor, A. Titterton

Rutherford Appleton Laboratory, Didcot, United Kingdom

K.W. Bell, A. Belyaev[63], C. Brew, R.M. Brown, D. Cieri, D.J.A. Cockerill, J.A. Coughlan, K. Harder, S. Harper, J. Linacre, K. Manolopoulos, E. Olaiya, D. Petyt, C.H. Shepherd-Themistocleous, A. Thea, I.R. Tomalin, T. Williams, W.J. Womersley

Imperial College, London, United Kingdom

R. Bainbridge, P. Bloch, J. Borg, S. Breeze, O. Buchmuller, A. Bundock, D. Colling, P. Dauncey, G. Davies, M. Della Negra, R. Di Maria, G. Hall, G. Iles, T. James, M. Komm, C. Laner, L. Lyons, A.-M. Magnan, S. Malik, A. Martelli, J. Nash[64], A. Nikitenko[7], V. Palladino, M. Pesaresi, D.M. Raymond, A. Richards, A. Rose, E. Scott, C. Seez, A. Shtipliyski, G. Singh, M. Stoye, T. Strebler, S. Summers, A. Tapper, K. Uchida, T. Virdee[17], N. Wardle, D. Winterbottom, J. Wright, S.C. Zenz

Brunel University, Uxbridge, United Kingdom

J.E. Cole, P.R. Hobson, A. Khan, P. Kyberd, C.K. Mackay, A. Morton, I.D. Reid, L. Teodorescu, S. Zahid

Baylor University, Waco, U.S.A.

K. Call, J. Dittmann, K. Hatakeyama, H. Liu, C. Madrid, B. McMaster, N. Pastika, C. Smith

Catholic University of America, Washington DC, U.S.A.

R. Bartek, A. Dominguez

The University of Alabama, Tuscaloosa, U.S.A.

A. Buccilli, S.I. Cooper, C. Henderson, P. Rumerio, C. West

Boston University, Boston, U.S.A.

D. Arcaro, T. Bose, D. Gastler, D. Pinna, D. Rankin, C. Richardson, J. Rohlf, L. Sulak, D. Zou

Brown University, Providence, U.S.A.

G. Benelli, X. Coubez, D. Cutts, M. Hadley, J. Hakala, U. Heintz, J.M. Hogan[65], K.H.M. Kwok, E. Laird, G. Landsberg, J. Lee, Z. Mao, M. Narain, S. Sagir[66], R. Syarif, E. Usai, D. Yu

JHEP02(2019)074

University of California, Davis, Davis, U.S.A.

R. Band, C. Brainerd, R. Breedon, D. Burns, M. Calderon De La Barca Sanchez, M. Chertok, J. Conway, R. Conway, P.T. Cox, R. Erbacher, C. Flores, G. Funk, W. Ko, O. Kukral, R. Lander, M. Mulhearn, D. Pellett, J. Pilot, S. Shalhout, M. Shi, D. Stolp, D. Taylor, K. Tos, M. Tripathi, Z. Wang, F. Zhang

University of California, Los Angeles, U.S.A.

M. Bachtis, C. Bravo, R. Cousins, A. Dasgupta, A. Florent, J. Hauser, M. Ignatenko, N. Mccoll, S. Regnard, D. Saltzberg, C. Schnaible, V. Valuev

University of California, Riverside, Riverside, U.S.A.

E. Bouvier, K. Burt, R. Clare, J.W. Gary, S.M.A. Ghiasi Shirazi, G. Hanson, G. Karapostoli, E. Kennedy, F. Lacroix, O.R. Long, M. Olmedo Negrete, M.I. Paneva, W. Si, L. Wang, H. Wei, S. Wimpenny, B.R. Yates

University of California, San Diego, La Jolla, U.S.A.

J.G. Branson, P. Chang, S. Cittolin, M. Derdzinski, R. Gerosa, D. Gilbert, B. Hashemi, A. Holzner, D. Klein, G. Kole, V. Krutelyov, J. Letts, M. Masciovecchio, D. Olivito, S. Padhi, M. Pieri, M. Sani, V. Sharma, S. Simon, M. Tadel, A. Vartak, S. Wasserbaech[67], J. Wood, F. Würthwein, A. Yagil, G. Zevi Della Porta

University of California, Santa Barbara — Department of Physics, Santa Barbara, U.S.A.

N. Amin, R. Bhandari, C. Campagnari, M. Citron, V. Dutta, M. Franco Sevilla, L. Gouskos, R. Heller, J. Incandela, A. Ovcharova, H. Qu, J. Richman, D. Stuart, I. Suarez, S. Wang, J. Yoo

California Institute of Technology, Pasadena, U.S.A.

D. Anderson, A. Bornheim, J.M. Lawhorn, N. Lu, H.B. Newman, T.Q. Nguyen, M. Spiropulu, J.R. Vlimant, R. Wilkinson, S. Xie, Z. Zhang, R.Y. Zhu

Carnegie Mellon University, Pittsburgh, U.S.A.

M.B. Andrews, T. Ferguson, T. Mudholkar, M. Paulini, M. Sun, I. Vorobiev, M. Weinberg

University of Colorado Boulder, Boulder, U.S.A.

J.P. Cumalat, W.T. Ford, F. Jensen, A. Johnson, E. MacDonald, T. Mulholland, R. Patel, A. Perloff, K. Stenson, K.A. Ulmer, S.R. Wagner

Cornell University, Ithaca, U.S.A.

J. Alexander, J. Chaves, Y. Cheng, J. Chu, A. Datta, K. Mcdermott, N. Mirman, J.R. Patterson, D. Quach, A. Rinkevicius, A. Ryd, L. Skinnari, L. Soffi, S.M. Tan, Z. Tao, J. Thom, J. Tucker, P. Wittich, M. Zientek

Fermi National Accelerator Laboratory, Batavia, U.S.A.

S. Abdullin, M. Albrow, M. Alyari, G. Apollinari, A. Apresyan, A. Apyan, S. Banerjee, L.A.T. Bauerdick, A. Beretvas, J. Berryhill, P.C. Bhat, K. Burkett, J.N. Butler, A. Canepa, G.B. Cerati, H.W.K. Cheung, F. Chlebana, M. Cremonesi, J. Duarte, V.D. Elvira, J. Freeman, Z. Gecse, E. Gottschalk, L. Gray, D. Green, S. Grünendahl, O. Gutsche,

JHEP02(2019)074

J. Hanlon, R.M. Harris, S. Hasegawa, J. Hirschauer, Z. Hu, B. Jayatilaka, S. Jindariani, M. Johnson, U. Joshi, B. Klima, M.J. Kortelainen, B. Kreis, S. Lammel, D. Lincoln, R. Lipton, M. Liu, T. Liu, J. Lykken, K. Maeshima, J.M. Marraffino, D. Mason, P. McBride, P. Merkel, S. Mrenna, S. Nahn, V. O'Dell, K. Pedro, C. Pena, O. Prokofyev, G. Rakness, L. Ristori, A. Savoy-Navarro[68], B. Schneider, E. Sexton-Kennedy, A. Soha, W.J. Spalding, L. Spiegel, S. Stoynev, J. Strait, N. Strobbe, L. Taylor, S. Tkaczyk, N.V. Tran, L. Uplegger, E.W. Vaandering, C. Vernieri, M. Verzocchi, R. Vidal, M. Wang, H.A. Weber, A. Whitbeck

University of Florida, Gainesville, U.S.A.

D. Acosta, P. Avery, P. Bortignon, D. Bourilkov, A. Brinkerhoff, L. Cadamuro, A. Carnes, D. Curry, R.D. Field, S.V. Gleyzer, B.M. Joshi, J. Konigsberg, A. Korytov, K.H. Lo, P. Ma, K. Matchev, H. Mei, G. Mitselmakher, D. Rosenzweig, K. Shi, D. Sperka, J. Wang, S. Wang, X. Zuo

Florida International University, Miami, U.S.A.

Y.R. Joshi, S. Linn

Florida State University, Tallahassee, U.S.A.

A. Ackert, T. Adams, A. Askew, S. Hagopian, V. Hagopian, K.F. Johnson, T. Kolberg, G. Martinez, T. Perry, H. Prosper, A. Saha, C. Schiber, R. Yohay

Florida Institute of Technology, Melbourne, U.S.A.

M.M. Baarmand, V. Bhopatkar, S. Colafranceschi, M. Hohlmann, D. Noonan, M. Rahmani, T. Roy, F. Yumiceva

University of Illinois at Chicago (UIC), Chicago, U.S.A.

M.R. Adams, L. Apanasevich, D. Berry, R.R. Betts, R. Cavanaugh, X. Chen, S. Dittmer, O. Evdokimov, C.E. Gerber, D.A. Hangal, D.J. Hofman, K. Jung, J. Kamin, C. Mills, M.B. Tonjes, N. Varelas, H. Wang, X. Wang, Z. Wu, J. Zhang

The University of Iowa, Iowa City, U.S.A.

M. Alhusseini, B. Bilki[69], W. Clarida, K. Dilsiz[70], S. Durgut, R.P. Gandrajula, M. Haytmyradov, V. Khristenko, J.-P. Merlo, A. Mestvirishvili, A. Moeller, J. Nachtman, H. Ogul[71], Y. Onel, F. Ozok[72], A. Penzo, C. Snyder, E. Tiras, J. Wetzel

Johns Hopkins University, Baltimore, U.S.A.

B. Blumenfeld, A. Cocoros, N. Eminizer, D. Fehling, L. Feng, A.V. Gritsan, W.T. Hung, P. Maksimovic, J. Roskes, U. Sarica, M. Swartz, M. Xiao, C. You

The University of Kansas, Lawrence, U.S.A.

A. Al-bataineh, P. Baringer, A. Bean, S. Boren, J. Bowen, A. Bylinkin, J. Castle, S. Khalil, A. Kropivnitskaya, D. Majumder, W. Mcbrayer, M. Murray, C. Rogan, S. Sanders, E. Schmitz, J.D. Tapia Takaki, Q. Wang

Kansas State University, Manhattan, U.S.A.

S. Duric, A. Ivanov, K. Kaadze, D. Kim, Y. Maravin, D.R. Mendis, T. Mitchell, A. Modak, A. Mohammadi, L.K. Saini

JHEP02(2019)074

Lawrence Livermore National Laboratory, Livermore, U.S.A.

F. Rebassoo, D. Wright

University of Maryland, College Park, U.S.A.

A. Baden, O. Baron, A. Belloni, S.C. Eno, Y. Feng, C. Ferraioli, N.J. Hadley, S. Jabeen, G.Y. Jeng, R.G. Kellogg, J. Kunkle, A.C. Mignerey, S. Nabili, F. Ricci-Tam, M. Seidel, Y.H. Shin, A. Skuja, S.C. Tonwar, K. Wong

Massachusetts Institute of Technology, Cambridge, U.S.A.

D. Abercrombie, B. Allen, V. Azzolini, A. Baty, G. Bauer, R. Bi, S. Brandt, W. Busza, I.A. Cali, M. D'Alfonso, Z. Demiragli, G. Gomez Ceballos, M. Goncharov, P. Harris, D. Hsu, M. Hu, Y. Iiyama, G.M. Innocenti, M. Klute, D. Kovalskyi, Y.-J. Lee, P.D. Luckey, B. Maier, A.C. Marini, C. Mcginn, C. Mironov, S. Narayanan, X. Niu, C. Paus, C. Roland, G. Roland, Z. Shi, G.S.F. Stephans, K. Sumorok, K. Tatar, D. Velicanu, J. Wang, T.W. Wang, B. Wyslouch

University of Minnesota, Minneapolis, U.S.A.

A.C. Benvenuti[†], R.M. Chatterjee, A. Evans, P. Hansen, J. Hiltbrand, Sh. Jain, S. Kalafut, M. Krohn, Y. Kubota, Z. Lesko, J. Mans, N. Ruckstuhl, R. Rusack, M.A. Wadud

University of Mississippi, Oxford, U.S.A.

J.G. Acosta, S. Oliveros

University of Nebraska-Lincoln, Lincoln, U.S.A.

E. Avdeeva, K. Bloom, D.R. Claes, C. Fangmeier, F. Golf, R. Gonzalez Suarez, R. Kamalieddin, I. Kravchenko, J. Monroy, J.E. Siado, G.R. Snow, B. Stieger

State University of New York at Buffalo, Buffalo, U.S.A.

A. Godshalk, C. Harrington, I. Iashvili, A. Kharchilava, C. Mclean, D. Nguyen, A. Parker, S. Rappoccio, B. Roozbahani

Northeastern University, Boston, U.S.A.

G. Alverson, E. Barberis, C. Freer, Y. Haddad, A. Hortiangtham, D.M. Morse, T. Orimoto, R. Teixeira De Lima, T. Wamorkar, B. Wang, A. Wisecarver, D. Wood

Northwestern University, Evanston, U.S.A.

S. Bhattacharya, J. Bueghly, O. Charaf, K.A. Hahn, N. Mucia, N. Odell, M.H. Schmitt, K. Sung, M. Trovato, M. Velasco

University of Notre Dame, Notre Dame, U.S.A.

R. Bucci, N. Dev, M. Hildreth, K. Hurtado Anampa, C. Jessop, D.J. Karmgard, N. Kellams, K. Lannon, W. Li, N. Loukas, N. Marinelli, F. Meng, C. Mueller, Y. Musienko[37], M. Planer, A. Reinsvold, R. Ruchti, P. Siddireddy, G. Smith, S. Taroni, M. Wayne, A. Wightman, M. Wolf, A. Woodard

The Ohio State University, Columbus, U.S.A.

J. Alimena, L. Antonelli, B. Bylsma, L.S. Durkin, S. Flowers, B. Francis, C. Hill, W. Ji, T.Y. Ling, W. Luo, B.L. Winer

JHEP02(2019)074

Princeton University, Princeton, U.S.A.

S. Cooperstein, P. Elmer, J. Hardenbrook, S. Higginbotham, A. Kalogeropoulos, D. Lange, M.T. Lucchini, J. Luo, D. Marlow, K. Mei, I. Ojalvo, J. Olsen, C. Palmer, P. Piroué, J. Salfeld-Nebgen, D. Stickland, C. Tully, Z. Wang

University of Puerto Rico, Mayaguez, U.S.A.

S. Malik, S. Norberg

Purdue University, West Lafayette, U.S.A.

A. Barker, V.E. Barnes, S. Das, L. Gutay, M. Jones, A.W. Jung, A. Khatiwada, B. Mahakud, D.H. Miller, N. Neumeister, C.C. Peng, S. Piperov, H. Qiu, J.F. Schulte, J. Sun, F. Wang, R. Xiao, W. Xie

Purdue University Northwest, Hammond, U.S.A.

T. Cheng, J. Dolen, N. Parashar

Rice University, Houston, U.S.A.

Z. Chen, K.M. Ecklund, S. Freed, F.J.M. Geurts, M. Kilpatrick, W. Li, B.P. Padley, R. Redjimi, J. Roberts, J. Rorie, W. Shi, Z. Tu, A. Zhang

University of Rochester, Rochester, U.S.A.

A. Bodek, P. de Barbaro, R. Demina, Y.t. Duh, J.L. Dulemba, C. Fallon, T. Ferbel, M. Galanti, A. Garcia-Bellido, J. Han, O. Hindrichs, A. Khukhunaishvili, E. Ranken, P. Tan, R. Taus

Rutgers, The State University of New Jersey, Piscataway, U.S.A.

A. Agapitos, J.P. Chou, Y. Gershtein, E. Halkiadakis, A. Hart, M. Heindl, E. Hughes, S. Kaplan, R. Kunnawalkam Elayavalli, S. Kyriacou, A. Lath, R. Montalvo, K. Nash, M. Osherson, H. Saka, S. Salur, S. Schnetzer, D. Sheffield, S. Somalwar, R. Stone, S. Thomas, P. Thomassen, M. Walker

University of Tennessee, Knoxville, U.S.A.

A.G. Delannoy, J. Heideman, G. Riley, S. Spanier

Texas A&M University, College Station, U.S.A.

O. Bouhali[73], A. Celik, M. Dalchenko, M. De Mattia, A. Delgado, S. Dildick, R. Eusebi, J. Gilmore, T. Huang, T. Kamon[74], S. Luo, R. Mueller, D. Overton, L. Perniè, D. Rathjens, A. Safonov

Texas Tech University, Lubbock, U.S.A.

N. Akchurin, J. Damgov, F. De Guio, P.R. Dudero, S. Kunori, K. Lamichhane, S.W. Lee, T. Mengke, S. Muthumuni, T. Peltola, S. Undleeb, I. Volobouev, Z. Wang

Vanderbilt University, Nashville, U.S.A.

S. Greene, A. Gurrola, R. Janjam, W. Johns, C. Maguire, A. Melo, H. Ni, K. Padeken, J.D. Ruiz Alvarez, P. Sheldon, S. Tuo, J. Velkovska, M. Verweij, Q. Xu

JHEP02(2019)074

University of Virginia, Charlottesville, U.S.A.

M.W. Arenton, P. Barria, B. Cox, R. Hirosky, M. Joyce, A. Ledovskoy, H. Li, C. Neu, T. Sinthuprasith, Y. Wang, E. Wolfe, F. Xia

Wayne State University, Detroit, U.S.A.

R. Harr, P.E. Karchin, N. Poudyal, J. Sturdy, P. Thapa, S. Zaleski

University of Wisconsin — Madison, Madison, WI, U.S.A.

M. Brodski, J. Buchanan, C. Caillol, D. Carlsmith, S. Dasu, I. De Bruyn, L. Dodd, B. Gomber[75], M. Grothe, M. Herndon, A. Hervé, U. Hussain, P. Klabbers, A. Lanaro, K. Long, R. Loveless, T. Ruggles, A. Savin, V. Sharma, N. Smith, W.H. Smith, N. Woods

†: Deceased
1: Also at Vienna University of Technology, Vienna, Austria
2: Also at IRFU, CEA, Université Paris-Saclay, Gif-sur-Yvette, France
3: Also at Universidade Estadual de Campinas, Campinas, Brazil
4: Also at Federal University of Rio Grande do Sul, Porto Alegre, Brazil
5: Also at Université Libre de Bruxelles, Bruxelles, Belgium
6: Also at University of Chinese Academy of Sciences, Beijing, China
7: Also at Institute for Theoretical and Experimental Physics, Moscow, Russia
8: Also at Joint Institute for Nuclear Research, Dubna, Russia
9: Also at Suez University, Suez, Egypt
10: Now at British University in Egypt, Cairo, Egypt
11: Now at Cairo University, Cairo, Egypt
12: Also at Department of Physics, King Abdulaziz University, Jeddah, Saudi Arabia
13: Also at Université de Haute Alsace, Mulhouse, France
14: Also at Skobeltsyn Institute of Nuclear Physics, Lomonosov Moscow State University, Moscow, Russia
15: Also at Tbilisi State University, Tbilisi, Georgia
16: Also at Ilia State University, Tbilisi, Georgia
17: Also at CERN, European Organization for Nuclear Research, Geneva, Switzerland
18: Also at RWTH Aachen University, III. Physikalisches Institut A, Aachen, Germany
19: Also at University of Hamburg, Hamburg, Germany
20: Also at Brandenburg University of Technology, Cottbus, Germany
21: Also at Institute of Physics, University of Debrecen, Debrecen, Hungary
22: Also at Institute of Nuclear Research ATOMKI, Debrecen, Hungary
23: Also at MTA-ELTE Lendület CMS Particle and Nuclear Physics Group, Eötvös Loránd University, Budapest, Hungary
24: Also at Indian Institute of Technology Bhubaneswar, Bhubaneswar, India
25: Also at Institute of Physics, Bhubaneswar, India
26: Also at Shoolini University, Solan, India
27: Also at University of Visva-Bharati, Santiniketan, India
28: Also at Isfahan University of Technology, Isfahan, Iran
29: Also at Plasma Physics Research Center, Science and Research Branch, Islamic Azad University, Tehran, Iran
30: Also at Università degli Studi di Siena, Siena, Italy
31: Also at Scuola Normale e Sezione dell'INFN, Pisa, Italy
32: Also at Kyunghee University, Seoul, Korea

JHEP02(2019)074

33: Also at International Islamic University of Malaysia, Kuala Lumpur, Malaysia
34: Also at Malaysian Nuclear Agency, MOSTI, Kajang, Malaysia
35: Also at Consejo Nacional de Ciencia y Tecnología, Mexico city, Mexico
36: Also at Warsaw University of Technology, Institute of Electronic Systems, Warsaw, Poland
37: Also at Institute for Nuclear Research, Moscow, Russia
38: Now at National Research Nuclear University 'Moscow Engineering Physics Institute' (MEPhI), Moscow, Russia
39: Also at St. Petersburg State Polytechnical University, St. Petersburg, Russia
40: Also at University of Florida, Gainesville, U.S.A.
41: Also at P.N. Lebedev Physical Institute, Moscow, Russia
42: Also at California Institute of Technology, Pasadena, U.S.A.
43: Also at Budker Institute of Nuclear Physics, Novosibirsk, Russia
44: Also at Faculty of Physics, University of Belgrade, Belgrade, Serbia
45: Also at INFN Sezione di Pavia [a], Università di Pavia [b], Pavia, Italy
46: Also at University of Belgrade, Faculty of Physics and Vinca Institute of Nuclear Sciences, Belgrade, Serbia
47: Also at National and Kapodistrian University of Athens, Athens, Greece
48: Also at Riga Technical University, Riga, Latvia
49: Also at Universität Zürich, Zurich, Switzerland
50: Also at Stefan Meyer Institute for Subatomic Physics (SMI), Vienna, Austria
51: Also at Adiyaman University, Adiyaman, Turkey
52: Also at Istanbul Aydin University, Istanbul, Turkey
53: Also at Mersin University, Mersin, Turkey
54: Also at Piri Reis University, Istanbul, Turkey
55: Also at Ozyegin University, Istanbul, Turkey
56: Also at Izmir Institute of Technology, Izmir, Turkey
57: Also at Marmara University, Istanbul, Turkey
58: Also at Kafkas University, Kars, Turkey
59: Also at Istanbul University, Faculty of Science, Istanbul, Turkey
60: Also at Istanbul Bilgi University, Istanbul, Turkey
61: Also at Hacettepe University, Ankara, Turkey
62: Also at Rutherford Appleton Laboratory, Didcot, United Kingdom
63: Also at School of Physics and Astronomy, University of Southampton, Southampton, United Kingdom
64: Also at Monash University, Faculty of Science, Clayton, Australia
65: Also at Bethel University, St. Paul, U.S.A.
66: Also at Karamanoğlu Mehmetbey University, Karaman, Turkey
67: Also at Utah Valley University, Orem, U.S.A.
68: Also at Purdue University, West Lafayette, U.S.A.
69: Also at Beykent University, Istanbul, Turkey
70: Also at Bingol University, Bingol, Turkey
71: Also at Sinop University, Sinop, Turkey
72: Also at Mimar Sinan University, Istanbul, Istanbul, Turkey
73: Also at Texas A&M University at Qatar, Doha, Qatar
74: Also at Kyungpook National University, Daegu, Korea
75: Also at University of Hyderabad, Hyderabad, India

JHEP02(2019)074